Available online at www.sciencedirect.com

ScienceDirect

Solar Energy 116 (2015) 144–164

SOLAR ENERGY

www.elsevier.com/locate/solener

Clear sky irradiances using REST2 and MODIS

Xiaohui Zhong *, Jan Kleissl

Center for Renewable Resources and Integration, Department of Mechanical and Aerospace Engineering, University of California, San Diego, 9500 Gilman Drive, La Jolla, CA 92093-0411, USA

Received 21 April 2014; received in revised form 15 March 2015; accepted 28 March 2015

Communicated by: Associate Editor David Renne

Abstract

In order to simulate historical Global Horizontal Irradiance (GHI) and Direct Normal Irradiance (DNI) solar resources, a method using MODIS level 3 (L3) daily satellite data as input to the REST2 clear sky model is presented to derive clear sky solar irradiance for California. MODIS L3 precipitable water (PW) and especially aerosol optical depth (AOD) were found to be significantly biased and were therefore calibrated based on AOD and PW from Aerosol Robotic Network (AERONET) ground monitoring sites.

For reference, MODIS input data was replaced by the following input data sources: 3 hourly PW and AOD from Monitoring Atmosphere Composition and Climate (MACC) and monthly climatological Linke Turbidity from Solar radiation Data (SoDa). Similarly, other clear sky models, specifically Ineichen and McClear, were also run for reference.

Validation was conducted using irradiance anomalies defined as the difference between irradiance and its 15 day moving average against ground measurement from California Irrigation Management Information System (CIMIS), National Renewable Energy Laboratory (NREL), and Integrated Surface Irradiance Study (ISIS) stations. It was found that the calibration of MODIS data markedly improves the accuracy of modeled GHI and DNI anomalies and REST2 clear sky model with calibrated MODIS data achieved the highest accuracy among all model and input data combinations. The improvement in accuracy of PW and AOD input data through calibration is relatively more important than the choice of clear sky model.

Keywords: REST2; MODIS; GHI; DNI

1. Introduction

Solar energy potential in a specific area depends on the local solar radiation resource. Since the atmospheric composition changes over minutes to seasonal and sometimes even annual time scales, solar resource assessment requires assessing the variation of solar radiation over multiple years (Gurtuna and Prevot, 2011). The ideal case is to use data from a well-maintained ground station near the site, but this scenario is unlikely since there are few such ground stations throughout the world. Alternatively, satellite data consisting of a clear sky model that is modulated by a cloud index (Gueymard and Thevenard, 2009; Gueymard and Wilcox, 2011; Mueller et al., 2004) allows nearly global coverage at fine spatial resolutions of one to a few km and temporal resolutions of 5–30 min (Gueymard, 2008; Miller et al., 2013; Perez et al., 2013; Renné et al., 2008). Therefore, satellite-derived solar irradiation is becoming more widely accepted and important to obtain financing for solar power projects (Gueymard, 2012a; Gurtuna and Prevot, 2011; Vignola et al., 2012).

One critical input to most semi-empirical satellite irradiance models is the clear sky irradiance. For example,

* Corresponding author. Tel.: +1 858 534 8087.
E-mail address: x6zhong@eng.ucsd.edu (X. Zhong).

http://dx.doi.org/10.1016/j.solener.2015.03.046
0038-092X/

Jamaly et al. (2012) showed that clear sky differences in a satellite based solar resource product, SolarAnywhere, explained most of the annual bias at sites throughout California. SolarAnywhere is a 1 km high resolution solar resource dataset and provides irradiation derived from Geostationary Operational Environmental Satellite (GOES) visible imagery at 1 km spatial and 30 min temporal resolution. REST2, METSTAT and Ineichen are considered the most accurate simple broadband clear sky irradiance models with an accuracy of a first class pyrheliometer (Gueymard, 2010; Reno et al., 2012). Lefèvre et al. (2013) developed an entirely physically-based clear sky model, McClear, with aerosol properties (primarily aerosol optical depth, AOD) as well as precipitable water (PW) provided by Monitoring Atmosphere Composition and Climate (MACC). MACC combines atmospheric modeling with earth observation data including both satellite and in-situ data, to provide aerosol properties and total column water vapor globally (Kaiser et al., 2012). In this paper, the accuracy of REST2, Ineichen, and McClear derived Global Horizontal Irradiance (GHI) and Direct Normal Irradiance (DNI) is compared.

The REST2 model accuracy depends mostly on the quality of the input data, especially the AOD and PW (Gueymard, 2012b; Reno et al., 2012). A sensitivity study and error analysis (Gueymard, 2003) demonstrated that the predicted irradiances are very sensitive to errors in the Angstrom turbidity coefficient that is calculated using AOD and Angstrom's wavelength Exponent. Generally, satellite observations of AOD over land are less accurate because variable surface reflectance, e.g. due to seasonal changes of vegetation, leaves a similar signature as variability in AOD (Hauser et al., 2005a). Currently, AOD data is available from e.g. the Advanced Very High Resolution Radiometer (AVHRR), Multi-angle Imaging Spectroradiometer (MISR), and Moderate Resolution Imaging Spectroradiometer (MODIS) satellite platforms. AVHRR has been in orbit continuously since 1981 but an AOD product over land has only recently been developed (Hauser et al., 2005b). MISR and MODIS were designed for AOD retrievals and provide robust retrievals of AOD over land. Statistical comparisons of coincident AOD over land between MISR and MODIS by Kahn et al. (2009) showed a correlation coefficient of 0.7. In addition, MODIS provides PW with typical errors estimated to range between 5% and 10% (Gao and Kaufman, 2003).

The combined land and ocean AOD MODIS level 3 (L3) daily (derived from one image at the overpass time) product is derived from the 0.55 μm channel of the Terra satellite and has been available since 2000. Ruiz-Arias et al. (2012) showed a reduction in the bias of GHI and DNI when the MODIS L3 AOD was input to the Goddard Space Flight Center (GSFC) shortwave scheme (Chou and Suarez, 1994) in the regional Weather Research and Forecasting (WRF) model. Ruiz-Arias et al. (2012) also compared GHI and DNI from GSFC against REST2 and showed that the GSFC is comparable to REST2 for GHI and less accurate than REST2 for DNI. In this paper, AOD, MODIS L3 daily PW, and Angstrom exponent are input into REST2 to model

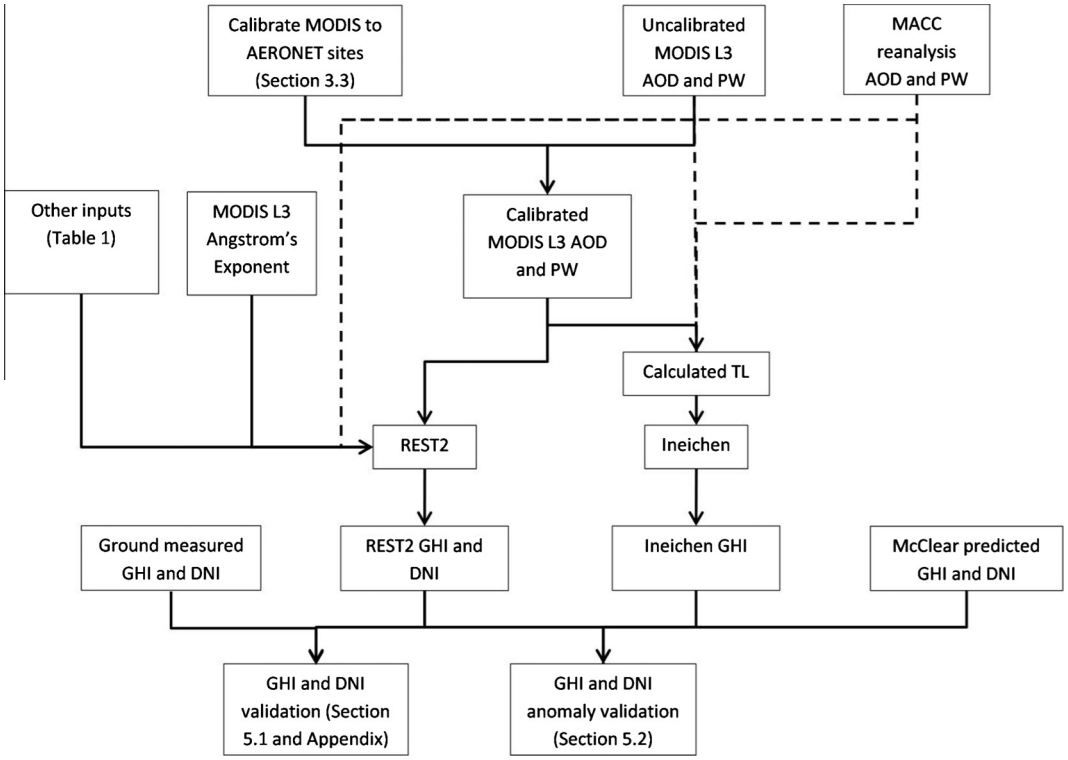

Fig. 1. Flow chart for the calibrations, model applications, and validations in the paper.

Table 1
REST2 inputs. Acronyms: NARR: North American Reanalysis, CIMIS: California Irrigation Management Information System; NREL: National Renewable Energy Laboratory; ISIS: Integrated Surface Irradiance Study.

Symbol	Quantity	Source
Albedo	Ground albedo	0.2 (default value), also could be obtained from satellite observations
p	Barometric pressure (mb)	NARR pressure vertically interpolated to station elevation
uo	Total ozone abundance (atm-cm), also called reduced ozone vertical pathlength	0.3 (default)
un	Total nitrogen dioxide abundance (atm-cm)	0.0002 (default)
w	Precipitable water (PW) (cm)	MODIS L3 or MACC reanalysis
α	Angstrom's wavelength Exponent	MODIS L3, see Eq. (1) or MACC reanalysis, see Eq. (4)
β	Angstrom's turbidity coefficient	MODIS L3 or MACC reanalysis input to Eq. (1)
$\tau_{a\lambda}$	AOD at wavelength ($\lambda = 0.55$ μm)	MODIS L3 or MACC reanalysis, see Eq. (1)
Pi01, Pi02	Aerosol single scattering albedo for spectral bands 1 and 2	0.95, 0.9 (default)
h	Elevation above mean sea level of the site	CIMIS/NREL/ISIS site elevation
Lat, Lon	Latitude, longitude	Center of MODIS L3 pixels, CIMIS/NREL/ISIS location
Year, month, day, hour LST	Time	Terra overpass time
Zone	Time zone	UTC-8

clear sky GHI and DNI. Since large biases in satellite PW and AOD were observed in California, MODIS PW and AOD were calibrated using ground data from 11 AERONET sites (Section 3). For comparison, MACC reanalysis AOD and PW as well as the derived Angstrom exponent from AOD at 0.55 and 1.24 μm (Lefèvre et al., 2013) are input to REST2 (without calibration). REST2 GHI and DNI and the Ineichen and McClear clear sky models are validated against GHI and DNI ground observations (Sections 4 and 5). GHI (DNI) anomalies were calculated by subtracting the moving average of GHI (DNI) on clear days within a 15 day period at the Terra overpass time (see Eq. (9) later). The flow chart for the analysis is shown in Fig. 1.

2. Data

2.1. REST2 input data

Table 1 shows the input parameters to REST2 (Gueymard, 2012b). The MODIS aboard two satellites, Terra and Aqua, measures atmospheric, oceanic, land surface, and cryospheric features of the entire Earth surface every 1–2 days (John, 2014; Remer et al., 2005). Over highly reflective surfaces such as deserts (e.g. Sahara) and snow covered mountains, MODIS data is not available (Ruiz-Arias et al., 2013). MODIS L3 atmospheric products are available over Daily, 8-Day, and Monthly temporal scales. In this paper, the MODIS L3 daily product is chosen, which becomes available approximately 20 days after measurement. The daily variability of clear sky solar radiation, which is important for solar power forecasting, cannot be demonstrated if only monthly data is used, since monthly AOD data captures only about half of the AOD variability (Gueymard, 2012c). Ruiz-Arias et al. (2013) concluded that MODIS L3 AOD is of sufficient quality to produce accurate GHI at the regional scale introducing an uncertainty of approximately 15% in DNI and less than 5% for GHI using REST2 (for AOD smaller than 0.5). In this paper we show that calibration (Section 3) makes the MODIS L3 AOD and PW more accurate.

Angstrom's turbidity coefficient is calculated using the linearization of Angstrom's law (Gueymard, 2008) which yields

$$\beta = \tau_{a\lambda}\lambda^{\alpha}, \tag{1}$$

from $\ln \tau_{a\lambda} = \ln \beta - \alpha \ln \lambda$ (see Table 1 for nomenclature). MODIS L3 AOD at $\lambda = 0.55$ μm is used for $\tau_{a\lambda}$ and α is the average MODIS L3 Angstrom Exponent (Land) for 0.47 and 0.66 μm. Both $\tau_{a\lambda}$ and α are derived from MODIS L2 data using quality assurance (QA) weighted statistics (Hubanks et al., 2008) as $\overline{d} = \sum_{i=1}^{n} w_i d_i / \sum_{i=1}^{n} w_i$, where $\overline{d}$ is MODIS L3 AOD or Angstrom exponent, d_i is the L2 AOD or Angstrom exponent, and w_i is the L2 QA value.[1] While REST2 treats the UV and visible (from 0.29 to 0.70 μm), and near-infrared (from 0.7 to 4 μm) bands separately (Gueymard, 2008), the α above is used for both bands because Angstrom exponents are only available for 0.47 and 0.66 μm.

Since the average MODIS pixel elevation is different from that of an AERONET ground site within the pixel, and, on average, AOD tends to decrease exponentially with altitude in the free troposphere the scale height (H_a) concept (Gueymard and Thevenard, 2009) is used to correct for elevation changes as

$$\mathrm{AOD}(h) = \mathrm{AOD}(h_0)\exp[(h_0 - h)/H_a], \tag{2}$$

where h_0 is the average elevation of the MODIS pixel derived from the 1 km by 1 km elevation data from the Weather Research and Forecasting (WRF) model within the MODIS pixel (see Table 4, Section 3); h is the elevation of the corresponding AERONET site; AOD(h_0) is the MODIS L3 AOD before elevation correction; and H_a is 2100 m for the six coastal (CalTech,

[1] 3: very good, 2: good confidence, 1: marginal confidence, and 0: no confidence.

El Segundo, La Jolla, Monterey, Trinidad Head and UCSB) and 2900 m for the six inland AERONET sites respectively. Similarly, MODIS L3 PW is corrected for elevation using Eq. (2) since water vapor is concentrated near the surface; H_w is 2100 m for coastal and 2500 m for inland AERONET sites respectively. We use the following elevation-corrected MODIS products from the Terra satellite: Aerosol Optical Thickness at 0.55 μm for both Ocean and Land (variable name: "Optical_Depth_Land_And_Ocean_Mean") and Precipitable Water Vapor (IR Retrieval, variable name: "Atmospheric_Water_Vapor_QA_Mean").

Pressure is temporally interpolated from 3 hourly pressure from the NCEP North American Regional Reanalysis (NARR) which assimilates comprehensive observational data. NARR pressure is extrapolated to the ground station elevation using

$$p_2 = p_1 e^{\left(\frac{g(h_2-h_1)}{RT}\right)}, \tag{3}$$

where p_2 and h_2 are the pressure and elevation of the ground station, p_1 is 3 hourly NARR pressure at the Terra overpass time, h_1 is the average elevation of the NARR pixel covering the ground station and R is the gas constant for dry air. NARR temperature is used as T which is a reasonable assumption because of small sensitivity and small height differences between ground stations and NARR pixels.

MACC reanalysis has been provided by the European Center for Medium-range Weather Forecast (ECMWF) since 2003. MODIS total aerosol optical depth is assimilated in the MACC reanalysis aerosol optical properties (Bellouin et al., 2013; Benedictow et al., 2014). However, unlike MODIS L3 which is an area average, MACC data are gridded point data (ECMWF, 2014). In this paper, MACC reanalysis 3 hourly data at 0.125° spatial resolution from MACC (2014) are used including "Total Aerosol Optical Depth at 550 nm", "Total Aerosol Optical Depth at 1240 nm" as well as "Total column water vapour". MACC Angstrom exponents are derived from AOD at 0.55 and 1.24 μm (Lefèvre et al., 2013) using

$$\alpha = -\frac{\ln\frac{\tau_{\lambda_1}}{\tau_{\lambda_2}}}{\ln\frac{\lambda_1}{\lambda_2}}, \tag{4}$$

where τ_{λ_1} and τ_{λ_2} optical thickness at $\lambda_1 = 0.55$ μm and $\lambda_2 = 1.24$ μm.

Scale height corrections are also applied to MACC AOD and PW data and the MACC grid point elevation (h_0 in Eq. (2)) is calculated from the MACC surface geopotential height and provided in Table 4.

2.2. Ineichen input data

Ineichen and Perez (2002) developed a clear sky model for GHI based on the Linke turbidity factor TL. In this paper the Ineichen model serves as a benchmark for other more complicated models. Ineichen (2008a) developed an expression for TL (for airmass equal to 2) as a function of atmospheric water vapor, aerosol optical depth, and altitude of the site as

$$TL = 3.91\exp\left(\frac{0.698p_0}{p}\right)\tau_{a0.55} + 0.376\ln(w) + \left[2 + 0.54\left(\frac{p_0}{p}\right) - 0.5\left(\frac{p_0}{p}\right)^2 + 0.16\left(\frac{p_0}{p}\right)^3\right], \tag{5}$$

where p_0 is the sea level atmospheric pressure. Eq. (5) showed negligible mean bias difference when evaluated against the radiative transfer model Modtran (Berk et al., 1989). Using Eq. (5), both MODIS and MACC data are converted to TL and input to Ineichen model. In addition the Ineichen model is run with climatological TL input data from Solar radiation Data (SoDa), a global TL database based on satellite data (Remund et al., 2003; SoDa, 2012).

2.3. McClear input data

A free Web service[2] delivers historical timeseries of global McClear clear sky irradiation with time steps as short as 1 min. The inputs to McClear are summarized in Table 2.

2.4. AERONET data

The AERONET (Aerosols Robotic Network, Holben et al., 1998, 2001) is a globally distributed network of identical robotically controlled ground-based sun photometers which measure atmospheric aerosol properties and compute AOD at three data quality levels: Level 1.0 (unscreened), Level 1.5 (cloud-screened), and Level 2.0 (cloud-screened and quality-assured). Since AERONET does not measure at 0.55 μm the comparison with MODIS L3 AOD at 0.55 μm requires that AOD at 0.55 μm is calculated from the level 2.0 AOD centered at 0.675 μm together with the level 2.0 Angstrom exponent derived from the 0.44 and 0.87 μm channels, consistent with Ruiz-Arias et al. (2013). Only AERONET sites (Table 4) that were continuously in operation for at least 190 days between 2009 and 2011 were selected. Three AERONET sites outside California are included because they are expected to be more representative of the eastern part of California, where considerable utility-scale solar power plant development is occurring.

2.5. CIMIS, NREL and ISIS validation data

The California Irrigation Management Information System (CIMIS) with 124 active weather stations is operated by the Department of Water Resources and has been operational since 1982 (CIMIS, 2009a). Each CIMIS

[2] http://www.soda-pro.com/web-services/radiation/mcclear (accessed 25.09.14).

Table 2
McClear inputs. In addition, solar zenith angle and other parameters related to geographical location and time are required. MCD43C1 are MODIS L3 16-day products at spatial resolution of 0.05° and provide three parameters fully describing the bidirectional reflectance distribution function (BRDF) (Lefèvre et al., 2013; Schaaf et al., 2002).

Symbol	Quantity	Source
uo and w	Total column content of ozone and water vapor	MACC reanalysis
Albedo	Ground albedo	Multiannual means of monthly averages of the BRDF parameters derived from 16 daily L3 MCD43C1 data over the period 2004–2011 (Blanc et al., 2014; Lefèvre et al., 2013)
	Vertical profile of temperature, pressure, density and volume mixing ratio for gases	USA Air Force Geophysics Laboratory (AFGL) data sets (Anderson et al., 1989)
h	Altitude	CIMIS/NREL/ISIS site elevation
$\tau_{a0.55}$	Aerosol optical depth at 0.55 μm	MACC reanalysis
α	Angstrom exponent	Derived from MACC reanalysis AOD at 0.55 μm and 1.24 μm using Eq. (4)
	Aerosol type	MACC reanalysis partial optical depths at 0.55 μm for dust, organic, sea salt, sulfate, and black carbon aerosol species (Benedetti et al., 2009)

station is equipped with a Li-Cor LI200S photodiode pyranometer accurate to ±5% based on sensor specifications (CIMIS, 2009b) and GHI is reported as an hourly average of 60 samples within the hour. A CIMIS station maintenance visit is called for every three or four weeks during the warmer months of the year and every five or six weeks during the cooler months (CIMIS, 2015). During the maintenance visit, the CIMIS stations sensors are checked for operation and accuracy and cleaned or replaced as needed. Since CIMIS stations are not centrally maintained, data quality issues exist for individual stations and this motivated a careful additional quality control by the authors. CIMIS provides quality control based on data averages, standard deviations, theoretical limits, and other procedures described by Meek and Hatfield (1994) and Eching and Moellenberndt (1998) and suspicious data is flagged and was removed for the analysis in this paper. Since this quality control is not sufficient to detect small measurement biases, Luoma and Kleissl (2012) visually examined data from each CIMIS station individually and excluded all questionable data. This manual quality control yielded 65 sites with higher quality data (Jamaly et al., 2012). However, post-processing corrections for air mass, temperature and spectral effects are not applied here (Geuder et al., 2008, 2009; King and Myers, 1997; Vignola, 2006).

Moreover, the GHI from the clear sky models is also compared with presumably more accurate ground measured GHI from the Integrated Surface Irradiance Study (ISIS, Hicks et al., 1996) site in Hanford and several National Renewable Energy Laboratory (NREL) supported sites shown in Table 3. ISIS uses Eppley Precision Spectral Pyranometers and a Normal Incidence Pyrheliometer to measure GHI and DNI directly and report it as 3 min averages. ISIS also provides the quality control flag following each measurement: a zero flag indicates a valid data point that passed all quality control checks; a flag greater than zero indicates that data failed at least one level of quality control. The NREL sites gather 1 minute DNI

Table 3
Geographical information on GHI and DNI validation sites: 4 NREL sites and 1 ISIS site in Hanford (last row). The instrument listed are Eppley Laboratory, Inc. Precision Spectral Pyranometer (PSP), LICOR LI-200 Pyranometer (LI-200), Kipp & Zonen CM3 Pyranometers, and Eppley Laboratory, Inc. Normal Incidence Pryheliometer (NIP), Irradiance Inc. Rotating Shadowband Radiometer (RSR), Eppley 8-48 pyranometer. For DNI 'calc' indicates that the DNI is calculated using measured GHI and diffuse horizontal irradiance (DHI) from a shaded instrument. The Nevada site at UNLV is chosen because it is close to MODIS pixel #46 (Fig. 2).

Site	Lat (°)	Lon (°)	Elevation (m)	MODIS pixel #	AERONET site	GHI Instrument	DNI Instrument	DHI Instrument
HSU	40.88	−124.08	36	2	Trinidad Head	PSP	Calc	PSP mounted under a manually-adjusted shadow band
SMUD	38.55	−121.24	51	15	Fresno	LI-200	Calc	LI-200 mounted on a RSR, and RSR band rotates every 30 s and blocks the sun
LMU	33.97	−118.42	27	36	UCSB	LI-200	Calc	LI-200 mounted on a RSR, and RSR band rotates every 30 s and blocks the sun
UNLV	36.06	−115.08	615	46	Goldstone	CM3	NIP mounted in an automatic sun-following tracker	Calc
Hanford	36.31	−119.63	73	29	Fresno	PSP	NIP	8-48 Pyranometer

and GHI and instruments are listed in Table 3. The NREL sites do not contain flags, but the data was visually examined for outliers by comparing irradiance on clear days against the REST2 + Calibrated MODIS clear sky model and found to be consistent. Since soiling is a particular concern for DNI measurements, the station environment were verified to be far away from large sources of soiling (highways, agricultural) and no evidence of rapid soiling was found in the clear sky data comparison. Maintenance records were requested for all sites and the records for Humboldt State University (HSU), Sacramento Municipal Utility District (SMUD), Loyola Marymount University (LMU), University of Nevada, Las Vegas (UNLV) and ISIS Hanford show frequent maintenance visits during the period of interest.

3. AOD and PW validation and calibration

3.1. Validation of MODIS L3 daily and MACC reanalysis 3 hourly AOD at 0.55 μm

It has been established that both MODIS AOD (Levy et al., 2010; Remer et al., 2005; Ruiz-Arias et al., 2013) and PW (Gao, 2003; King et al., 2003; Li et al., 2003; Prasad and Singh, 2009) are often biased especially over high albedo sites and should be calibrated before application. AOD and PW are calibrated against AOD and PW at 11 AERONET sites (Fig. 2).

Table 5 compares MODIS L3 and MACC reanalysis with AERONET AOD at 0.55 μm using mean bias error (MBE), mean absolute error (MAE), and Pearson's correlation coefficient. Relative errors (rMBE and rMAE) are obtained by dividing by the annual average AOD.

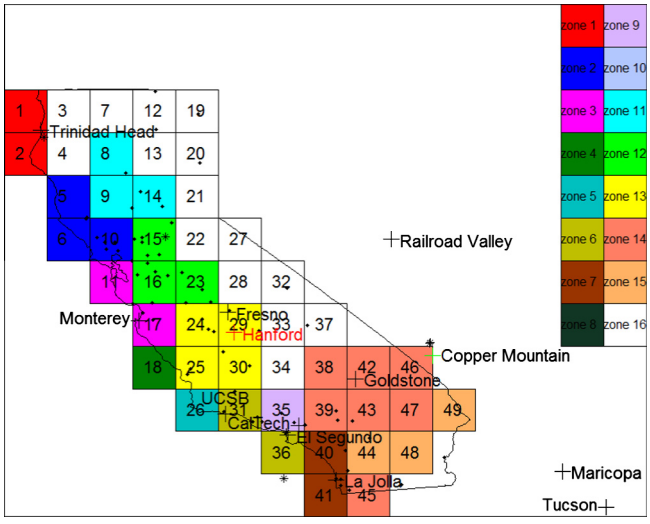

Fig. 2. MODIS pixels numbered and grouped into 16 climate zones (color) with 65 high quality CIMIS stations overlaid (dots), 11 AERONET sites (black crosses), 4 NREL sites (black stars) and one ISIS sites in Hanford (red cross). For the MODIS pixels that contain more than one climate zone, the climate zone associated with the largest areal coverage is used. Zone 8 is so small that it is not shown. (For interpretation of the references to color in this figure legend, the reader is referred to the web version of this article.)

$$\mathrm{MBE} = \frac{1}{N}\sum_{i=1}^{N}(\mathrm{MODIS} - \mathrm{AERONET}) \tag{6}$$

$$\mathrm{MAE} = \frac{1}{N}\sum_{i=1}^{N}|\mathrm{MODIS} - \mathrm{AERONET}| \tag{7}$$

The AODs in the southwestern US are generally small with annual means smaller than 0.1 and will affect GHI only by less than 5% (Ruiz-Arias et al., 2013). The inland sites tend to have smaller AODs with the exception of Fresno that may be impacted by agricultural activity. Overall we observe a significant correlation between MODIS and AERONET (0.39–0.73), but MODIS is usually biased large consistent with Ruiz-Arias et al. (2013) and (Levy et al., 2010), which may be attributed to the misrepresentation of the land surface and/or assumed aerosol properties in the algorithm (Levy et al., 2010). Especially, at the inland AERONET stations (e.g. at Goldstone, Fig. 3) MODIS AOD is up to 7 times larger than AERONET AOD. MODIS AOD biases are generally large with the exception of a few coastal sites (e.g. CalTech, Trinidad Head and UCSB). Clearly, uncalibrated MODIS AOD is not a suitable input to solar resource models. However, due to the significant correlation a linear regression fit could remove much of the errors while retaining information on the day-to-day variability in AOD.

Similarly, MACC AOD is biased large by 128%, on average, which is not surprising since MODIS AOD is assimilated into MACC. Our results are consistent with Benedictow et al. (2014) who performed evaluation of the MACC reanalysis AOD against AERONET level 2.0 AOD for 2003–2012. Their Fig. 3.5.2 illustrates high biases in several years (2003–2012) in western, central and northern North America. Although the average correlation between MACC and AERONET is only 0.34, higher correlations are expected in other parts of the world.

3.2. Validation of MODIS L3 daily and MACC reanalysis 3 hourly PW

Table 6 compares the MODIS L3 and MACC reanalysis PW against the 11 AERONET sites. MODIS overestimates at all sites, but the largest errors and relative errors come from the coastal sites (Fig. 4) with rMBEs greater than 30%, presumably due to a large part of the respective MODIS pixels covering the ocean. MACC PW is more accurate than MODIS PW in terms of average MBE and MAE. Overall, the correlation coefficients are mostly larger than 0.8, so both MODIS and MACC PW are well correlated with AERONET PW. The PW and AOD analysis demonstrates that the MODIS products are valuable inputs to clear sky solar resource models if bias and most of the MAE are removed through calibration against ground data.

Table 4
Geographical information on AERONET sites used for calibrating MODIS data. All sites are in California unless otherwise indicated. The elevation column indicates the AERONET site elevation above mean sea level (MSL), the average elevation of MODIS L3 pixel and MACC grid point elevation. The year column indicates what AERONET time period is used to calibrate MODIS data (ground measured GHI will be compared against the clear sky models for the same time period later). The MODIS latitude and longitude are for the center of the MODIS pixel containing the AERONET site and MACC latitude and longitude are for the MACC grid point closest to the AERONET site and the respective distances to the AERONET site are also provided.

AERONET Site	Lat (°)	Lon (°)	Elevation (m MSL)	Year	MODIS				MACC			
					Lat (°)	Long (°)	Elevation (m)	Distance (km)	Lat (°)	Long (°)	Elevation (m)	Distance (km)
CalTech	34.14	−118.13	260	2011	34.5	−118.5	731	53	34.125	−118.125	503.94	1.34
El Segundo	33.91	−118.38	25	2011	33.5	−118.5	9	47	33.875	−118.375	331.73	4.27
Fresno	36.78	−119.77	0	2011	36.5	−119.5	205	40	36.75	−119.75	591.44	4.11
Goldstone	35.23	−116.79	1100	2011	35.5	−116.5	678	40	35.25	−116.75	832.59	4.26
La Jolla	32.87	−117.25	115	2011	32.5	−117.5	13	47	32.875	−117.25	450.35	0.56
Monterey	36.59	−121.86	50	2009	36.5	−121.5	337	33	36.625	−121.875	201.47	3.98
Trinidad Head	41.05	−124.15	105	2011	41.5	−124.5	30	58	41	−124.125	590.71	6.39
UCSB	34.42	−119.85	33	2011	34.5	−119.5	626	33	34.375	−119.875	409.85	5.23
Railroad Valley (NV)	38.5	−115.96	1435	2010	38.5	−115.5	1813	40	38.5	−116	1944.21	3.34
Maricopa (AZ)	33.07	−111.97	360	2010	33.5	−111.5	767	65	33.125	−112	541.95	6.75
Tucson (AZ)	32.23	−110.95	779	2010	32.5	−110.5	1237	52	32.25	−111	1027.54	4.81

Table 5
Comparison of MODIS L3 and MACC reanalysis AOD (unitless) at 0.55 μm against AERONET AOD at 0.55 μm. 'r' indicates the relative error. Note that MBE = MAE for several stations, since MODIS AOD is always larger than AERONET there. See Table 4 for MODIS pixel and MACC grid point coordinates.

AERONET site	Annual Mean	MODIS L3					MACC				
		MBE	rMBE (%)	MAE	rMAE (%)	Cor	MBE	rMBE (%)	MAE	rMAE (%)	Cor
CalTech	0.08	0.01	9	0.05	64	0.44	0.07	95	0.09	112	0.21
El Segundo	0.09	0.08	82	0.09	97	0.56	0.06	63	0.08	84	0.19
Fresno	0.12	0.01	5	0.06	49	0.56	0.04	37	0.07	60	0.33
Goldstone	0.04	0.28	666	0.28	666	0.54	0.10	232	0.10	234	0.42
La Jolla	0.09	0.03	28	0.04	42	0.73	0.08	85	0.09	96	0.29
Monterey	0.08	−0.04	−49	0.05	69	0.43	0.05	63	0.06	75	0.43
Trinidad Head	0.08	0.00	3	0.04	52	0.39	0.04	49	0.05	60	0.51
UCSB	0.07	0.00	3	0.05	65	0.47	0.08	112	0.08	118	0.35
Railroad Valley	0.05	0.29	627	0.29	627	0.45	0.11	227	0.11	230	0.36
Maricopa	0.07	0.15	222	0.15	222	0.55	0.11	172	0.11	172	0.24
Tucson	0.04	0.13	364	0.13	364	0.71	0.10	278	0.10	278	0.41
Average	0.07	0.08	178	0.11	211	0.53	0.08	128	0.09	138	0.34

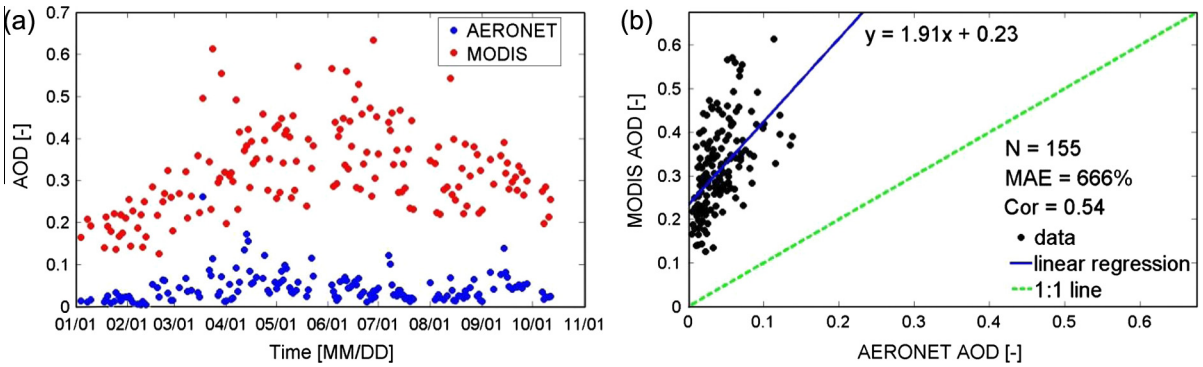

Fig. 3. Comparison of AOD at 0.55 μm from MODIS and AERONET at Goldstone (Tables 4 and 5) in 2011. Each datapoint represents one day, where AERONET data is averaged over ±30 min around the Terra overpass time. Data for days with clouds within ±30 min of the Terra overpass time were removed. There is no quality assured AERONET level 2.0 AOD from Goldstone after Oct 13, 2011.

Table 6
Comparison of MODIS L3 and MACC reanalysis PW against AERONET PW.

AERONET site	Annual Mean (cm)	MODIS					MACC				
		MBE (cm)	rMBE (%)	MAE (cm)	rMAE (%)	Cor	MBE (cm)	rMBE (%)	MAE (cm)	rMAE (%)	Cor
CalTech	1.00	0.50	50	0.51	51	0.81	0.09	9	0.17	17	0.92
El Segundo	1.18	0.61	52	0.62	53	0.73	−0.03	−2	0.18	15	0.91
Fresno	1.64	0.02	1	0.29	18	0.86	0.01	0	0.21	13	0.90
Goldstone	0.89	0.06	7	0.17	19	0.92	0.13	16	0.16	19	0.94
La Jolla	1.35	0.66	49	0.67	50	0.89	0.02	2	0.16	13	0.94
Monterey	1.40	0.46	33	0.48	34	0.82	0.01	0	0.14	10	0.93
Trinidad Head	1.10	0.41	37	0.45	41	0.76	0.03	3	0.13	12	0.95
UCSB	1.33	0.77	58	0.77	58	0.85	0.07	6	0.20	16	0.89
Railroad Valley	0.75	0.20	26	0.3	39	0.87	0.40	54	0.42	57	0.82
Maricopa	0.95	0.08	8	0.21	22	0.80	0.40	43	0.42	46	0.67
Tucson	0.90	0.19	21	0.25	28	0.88	0.50	57	0.51	58	0.88
Average	1.14	0.36	31	0.43	38	0.84	0.15	17	0.24	25	0.89

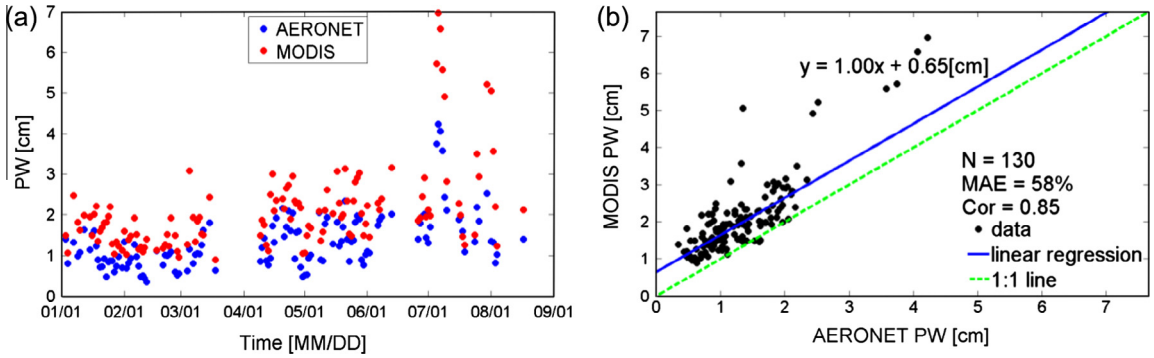

Fig. 4. Comparison of MODIS and AERONET PW at UCSB in 2011. Data for days with clouds within the ±30 min of the Terra overpass time were removed. There is no quality assured AERONET level 2.0 PW from UCSB after Aug 17, 2011.

3.3. Calibration of MODIS L3 daily AOD and PW

California has a great diversity of climates which varies from Mediterranean to subarctic. For building energy modeling, California is typically divided into 16 Climate Zones (Pacific Gas and Electric Company, 2006). We assume that the California Climate Zones are representative of atmospheric conditions including PW and AOD. Therefore when applying MODIS calibrations, rather than using the nearest AERONET site, the climate zones are used to match MODIS calibrations from the 11 AERONET sites to the 49 MODIS L3 pixels in California (Fig. 2). As shown in Figs. 3 and 4 a linear regression is applied to the AOD and PW data from MODIS versus AERONET in Tables 5 and 6. One regression is obtained per MODIS pixel using the AERONET sites assigned in Table 7 and the regression is then applied to the MODIS data across the entire year. Also, the MACC reanalysis AOD and PW could be calibrated in a similar way as MODIS products.

Table 7
Climate zone, MODIS pixels and corresponding AERONET site used for calibrating the MODIS pixels.

Climate zone	MODIS pixel	AERONET site
1	1, 2	Trinidad Head
2	5, 6, 10	Trinidad Head
3	11, 17	Monterey
4	18	Monterey
5	26	UCSB
6	31, 36	UCSB
7	40, 41	La Jolla
9	35	CalTech
11	8, 9, 14	Fresno
12	15, 16, 23	Fresno
13	24, 25, 29, 30	Fresno
14	38, 39, 42, 43, 45, 46, 47	Goldstone
15	44, 48, 49	Goldstone
16	3, 4, 7, 12, 13	Trinidad Head
16	19, 20, 21, 22, 27, 28, 32, 33, 34, 37	Railroad Valley

4. GHI and DNI validation methods

The GHI and DNI outputs of the following clear sky models were compared with GHI and DNI from ground measurements at the Terra overpass time: (a) REST2 with (i) calibrated MODIS, (ii) uncalibrated MODIS, and (iii) MACC reanalysis. (b) Ineichen with (i) derived *TL* from

uncalibrated and calibrated MODIS L3 data, (ii) monthly climatological Linke turbidity from the SoDa database, and (iii) derived *TL* from MACC reanalysis data. (c) 1 min timeseries of McClear irradiation (integral of solar irradiance over a time period with units of W h/m^2) are downloaded and converted to irradiance (has units W/m^2) for comparison. Fig. 1 shows a flowchart of all permutations of input data and clear sky models.

The CIMIS station closest to the center of the MODIS pixel or the MACC grid point is used for validation. Since the clear sky models provide GHI in clear conditions, data in cloudy conditions within ±30 min of the Terra overpass time (1000–1100 PST) are removed by retaining only data with a CIMIS clear sky index for the hourly interval of larger than 0.9 and smaller than 1.1. The clear sky index is calculated using clear sky GHI from the Ineichen model (Ineichen, 2008b) with Linke Turbidity monthly climatological averages from the SoDa Service

$$k_t(t) = \frac{\mathrm{GHI}(t)}{\text{Ineichen GHI}(t)} \tag{8}$$

Outliers in the data meeting the average clear sky index criteria were removed if they differed by more than three standard deviations from the annual average GHI. Since the NREL and ISIS sites report 1 min and 3 min, respectively, GHI and diffuse horizontal irradiance (DHI) an algorithm that also considers temporal standard deviations in clear sky index is applied to select clear periods (Long and Ackerman, 2000).

GHI comparisons result in large correlations due to the underlying annual and daily cycle of solar angles. Therefore, Gueymard (2012c) used the relative difference between annual average GHI and long-term average GHI to define an annual GHI anomaly. Similarly, to test the day-to-day variability caused by differences in atmospheric composition, the GHI anomaly ΔGHI is here calculated by subtracting the 15 day moving average (only using clear days within a 15 day period at the Terra overpass time) from the GHI at Terra overpass time on the each day of interest (Eq. (9)).

$$\Delta\mathrm{GHI}(t) = \mathrm{GHI}(t) - \frac{1}{15}\sum_{i=t-7\text{days}}^{t+7\text{days}} \mathrm{GHI}(i), \tag{9}$$

where t is the Terra overpass time on the day of interest and i is the clear sky Terra overpass time on one of the days within the 15 day period. For DNI, REST2 and McClear are compared against 4 NREL and 1 ISIS site for 2009–2011 and Eq. (9) is also applied to calculate DNI anomalies ΔDNI. Quality control was conducted by (i) eliminating DNI smaller than 100 W m^{-2} (since only clear conditions were of interest), (ii) eliminating flagged (Section 2.5) ISIS measurements, and (iii) applying a triplet stability criterion by requiring that 3 subsequent measurements (for NREL 1 min averages and for ISIS 3 min averages) vary by less than 3%, (iv) eliminating values that differed by more than three standard deviations from the mean, and (v) visually detecting and removing outliers in graphs of the fraction of direct horizontal to GHI.

5. Validation

5.1. Global horizontal irradiance

Fig. 5a shows a typical timeseries of CIMIS, REST2 + uncalibrated MODIS, and Ineichen + SoDa predicted GHI. By design the climatological Ineichen + SoDa model does not capture the day-to-day GHI variability, while the REST2 + uncalibrated MODIS predicted GHI captures the range of CIMIS daily variability reasonably well except for when the MODIS AOD is biased significantly. For reference, non-anomaly GHI results for relatively higher quality and better maintained NREL and ISIS stations are compared in Tables A-1–A-3 (Appendix A).

5.2. Global horizontal irradiance anomaly

We now focus on anomaly results which removes effects of the diurnal cycle resulting in smaller but more relevant correlation coefficients and error metrics (Tables 8.1 and

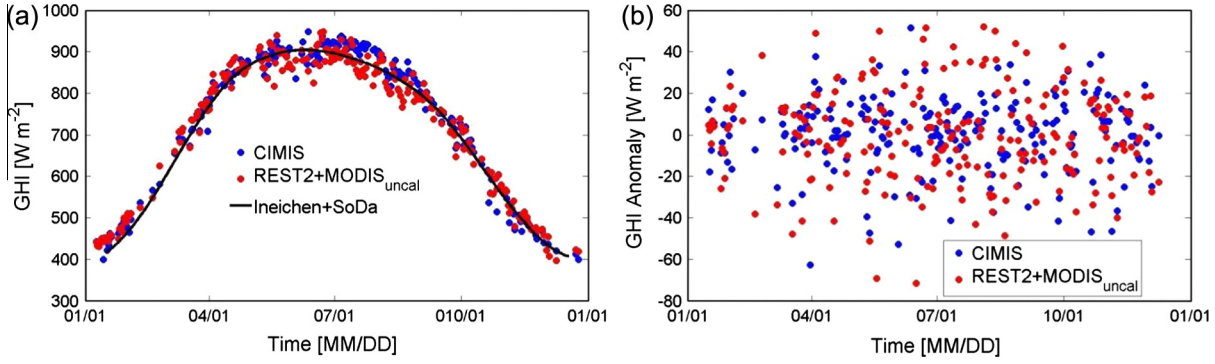

Fig. 5. Timeseries of CIMIS measured, REST2 + uncalibrated MODIS predicted and Ineichen + SoDa predicted GHI (a) and GHI anomaly (b) for uncalibrated MODIS AOD at 0.55 μm and PW at MODIS pixel #11 and CIMIS station 170 in coastal northern California in 2009. Days with clouds within the ±30 min of the Terra overpass time were removed.

Table 8.1
rMAE of REST2 (columns 5, 6, and 11), Ineichen (columns 7–9, and 12) and McClear (column 10) predicted GHI anomalies against CIMIS, NREL and ISIS measured GHI anomalies. Anomalies were calculated by subtracting 15 day moving averages (Eq. (9)). The other columns are (1) the MODIS pixel number, (2) the CIMIS station ID (rows 2–28) and names of NREL (rows 29–32) and ISIS sites (row 33), (3) the AERONET site that was used to calibrate MODIS AOD and PW, and (4) the distance (km) between the center of the MODIS pixel and the ground station. Further, "cal_" means that MODIS data was "calibrated" (Section 3). All errors are relative errors normalized by annual average ground measured GHI.

#	ID	AERONET	Distance (km)	REST2 + MODIS		Ineichen + MODIS		Ineichen + SoDa	McClear	REST2 + MACC	Ineichen + MACC
				rMAE (%)	cal_rMAE (%)	rMAE (%)	cal_rMAE (%)	rMAE (%)	rMAE (%)	rMAE (%)	rMAE (%)
5	85	Trinidad Head	65	1.81	1.61	1.83	1.39	1.54	1.73	1.89	1.84
6	106	Trinidad Head	64	2.32	1.40	2.52	1.25	1.35	1.77	1.84	1.66
8	8	Fresno	58	2.59	1.98	2.62	1.91	2.09	2.19	2.43	2.65
9	32	Fresno	51	2.32	1.70	2.61	1.66	1.88	2.00	2.13	2.30
10	77	Trinidad Head	11	2.34	1.71	2.12	1.54	1.75	2.21	2.31	1.92
11	170	Monterey	70	2.11	1.60	1.96	1.49	1.78	2.00	1.89	1.78
12	43	Railroad Valley	48	2.35	2.09	2.70	1.55	1.57	2.06	2.28	2.40
14	12	Fresno	30	2.17	1.85	2.23	1.93	2.15	2.21	2.18	2.54
15	6	Fresno	25	2.03	1.63	2.28	2.07	2.28	2.14	2.08	2.51
16	167	Fresno	26	1.87	1.06	2.14	1.70	1.83	1.79	1.81	2.18
17	89	Monterey	13	2.75	1.84	2.03	1.41	1.81	2.23	2.19	1.81
19	90	Railroad Valley	8	2.30	1.71	1.97	1.67	1.82	2.11	2.50	2.39
20	57	Railroad Valley	24	2.13	1.95	2.36	1.98	2.20	2.25	2.45	2.59
23	194	Fresno	39	2.22	1.39	2.26	1.43	1.56	1.74	1.87	1.90
24	190	Fresno	26	2.32	1.64	2.43	1.73	2.01	1.96	2.00	2.14
25	160	Fresno	27	2.25	1.55	2.43	1.61	1.67	1.86	2.00	1.86
29	80	Fresno	42	2.48	1.75	2.53	1.85	2.00	1.96	2.16	3.22
30	5	Fresno	20	2.56	1.70	2.83	1.94	2.16	2.17	2.23	2.34
31	156	UCSB	41	2.44	2.02	2.60	2.14	2.32	2.47	2.46	3.05
32	35	Railroad Valley	18	1.88	1.38	2.30	1.39	1.43	1.35	1.98	1.77
35	152	CalTech	54	2.17	1.68	2.20	1.66	1.82	2.20	2.27	2.60
37	183	Railroad Valley	38	1.82	1.52	3.04	1.50	1.59	1.65	2.42	2.21
39	192	Goldstone	37	1.90	1.21	1.81	1.40	1.61	1.12	1.79	1.66
41	184	La Jolla	42	2.52	2.21	2.62	2.07	2.10	2.18	2.54	2.55
43	199	Goldstone	45	1.50	1.14	1.39	1.17	1.26	1.04	1.66	1.23
44	118	Goldstone	38	2.43	1.45	2.46	1.75	2.09	2.09	2.17	2.36
45	147	Goldstone	44	2.23	1.67	2.39	1.76	2.08	2.25	2.27	2.31
2	HSU	Trinidad Head	55	1.28	0.88	1.45	0.90	1.17	0.93	1.23	1.09
15	SMUD	Fresno	23	1.41	0.85	1.46	0.94	1.21	1.44	1.66	1.62
36	LMU	UCSB	52	2.51	1.17	3.52	1.14	1.22	1.39	1.62	1.83
46	UNLV	Goldstone	73	1.37	1.11	1.80	1.17	1.45	1.62	1.69	2.16
29	Hanford	Fresno	24	2.26	1.44	2.22	1.42	1.42	1.50	1.67	1.66
Max				2.75	2.21	3.52	2.14	2.32	2.47	2.54	3.22
Min				1.28	0.85	1.39	0.90	1.17	0.93	1.23	1.09
Average				2.14	1.56	2.28	1.58	1.76	1.86	2.05	2.13

8.2 and Figs. 5b, 7, 8). Anomaly errors better illustrate model performance as they are independent of long-term measurement biases or erroneous low frequency signals in the sensor data, e.g. from soiling. Given that rMBE of anomalies is negligible by design, the rMBE comparison is not included in Table 8. The rMAE comparison in Table 8.1 shows that the REST2 and Ineichen models with calibrated MODIS exhibit the smallest average relative rMAEs of 1.56% and 1.58% respectively, and Ineichen + uncalibrated MODIS produces the largest error. Since AODs in the California are generally small (Table 4) clear sky GHI is more sensitive to absorption by PW, which explains why REST2 and Ineichen with calibrated MODIS have smaller rMAEs than those of REST2 and Ineichen with uncalibrated MODIS. Ineichen + SoDa, the only model with monthly climatological input data, shows smaller rMAE than Ineichen + uncalibrated MODIS, but also the lowest correlation (Table 8.2) since the day-to-day variability and deviations from the climatology are not considered. Comparing REST2 and Ineichen with the same input data, REST2 outperforms the rMAE of Ineichen.

Since REST2 with calibrated MODIS achieves the smallest rMAE, we proceed to evaluate the impact of MODIS calibration on the results. Fig. 6 compares REST2 predicted GHI anomaly for uncalibrated and

Table 8.2
Correlation coefficient (Cor) of REST2 (columns 5, 6, and 11), Ineichen (columns 7–9 and 12) and McClear predicted GHI anomalies (column 10) against CIMIS, NREL and ISIS measured GHI anomalies.

#	ID	AERONET	Distance (km)	REST2 + MODIS		Ineichen + MODIS		Ineichen + SoDa	McClear	REST2 + MACC	Ineichen + MACC
				Cor	cal_Cor	Cor	cal_Cor	Cor	Cor	Cor	Cor
5	85	Trinidad Head	65	0.46	0.40	0.39	0.44	0.22	0.45	0.47	0.39
6	106	Trinidad Head	64	0.52	0.58	0.37	0.63	0.53	0.54	0.67	0.64
8	8	Fresno	58	0.45	0.47	0.47	0.47	0.20	0.37	0.41	0.33
9	32	Fresno	51	0.53	0.54	0.47	0.52	0.22	0.43	0.49	0.36
10	77	Trinidad Head	11	0.48	0.58	0.47	0.53	0.26	0.39	0.44	0.45
11	170	Monterey	70	0.52	0.49	0.49	0.52	0.17	0.44	0.52	0.49
12	43	Railroad Valley	48	0.46	0.39	−0.16	0.27	0.36	0.51	0.50	0.17
14	12	Fresno	30	0.65	0.65	0.52	0.49	0.13	0.41	0.51	0.34
15	6	Fresno	25	0.48	0.46	0.42	0.44	0.16	0.42	0.52	0.38
16	167	Fresno	26	0.61	0.71	0.39	0.47	0.32	0.51	0.64	0.36
17	89	Monterey	13	0.28	0.37	0.60	0.64	0.25	0.33	0.41	0.46
19	90	Railroad Valley	8	0.31	0.44	0.32	0.54	0.46	0.49	0.43	0.38
20	57	Railroad Valley	24	0.70	0.64	0.73	0.66	0.45	0.48	0.49	0.40
23	194	Fresno	39	0.53	0.57	0.45	0.49	0.23	0.46	0.56	0.46
24	190	Fresno	26	0.54	0.61	0.50	0.56	0.21	0.48	0.54	0.45
25	160	Fresno	27	0.44	0.46	0.32	0.39	0.21	0.46	0.49	0.43
29	80	Fresno	42	0.43	0.46	0.36	0.39	0.14	0.44	0.49	0.13
30	5	Fresno	20	0.49	0.50	0.42	0.44	0.10	0.40	0.49	0.33
31	156	UCSB	41	0.35	0.34	0.32	0.37	0.19	0.28	0.38	0.23
32	35	Railroad Valley	18	0.37	0.44	0.29	0.44	0.33	0.47	0.38	0.39
35	152	CalTech	54	0.55	0.58	0.44	0.50	0.23	0.27	0.42	0.22
37	183	Railroad Valley	38	0.35	0.37	0.01	0.37	0.62	0.51	0.54	0.51
39	192	Goldstone	37	0.53	0.60	0.36	0.53	0.20	0.66	0.53	0.40
41	184	La Jolla	42	0.37	0.42	0.22	0.30	0.17	0.39	0.46	0.35
43	199	Goldstone	45	0.39	0.48	0.31	0.47	0.37	0.56	0.48	0.48
44	118	Goldstone	38	0.54	0.61	0.34	0.46	0.10	0.47	0.57	0.38
45	147	Goldstone	44	0.47	0.54	0.36	0.51	0.11	0.35	0.47	0.31
2	HSU	Trinidad Head	55	0.74	0.76	0.60	0.69	0.31	0.84	0.77	0.73
15	SMUD	Fresno	23	0.73	0.73	0.64	0.71	0.31	0.63	0.68	0.60
36	LMU	UCSB	52	0.39	0.59	0.22	0.52	0.41	0.55	0.67	0.48
46	UNLV	Goldstone	73	0.68	0.70	0.51	0.66	0.24	0.64	0.72	0.57
29	Hanford	Fresno	24	0.51	0.59	0.50	0.57	0.49	0.57	0.64	0.57
Max				0.74	0.76	0.73	0.71	0.62	0.84	0.77	0.73
Min				0.28	0.34	0.01	0.27	0.10	0.27	0.38	0.13
Average				0.50	0.53	0.40	0.50	0.27	0.48	0.52	0.41

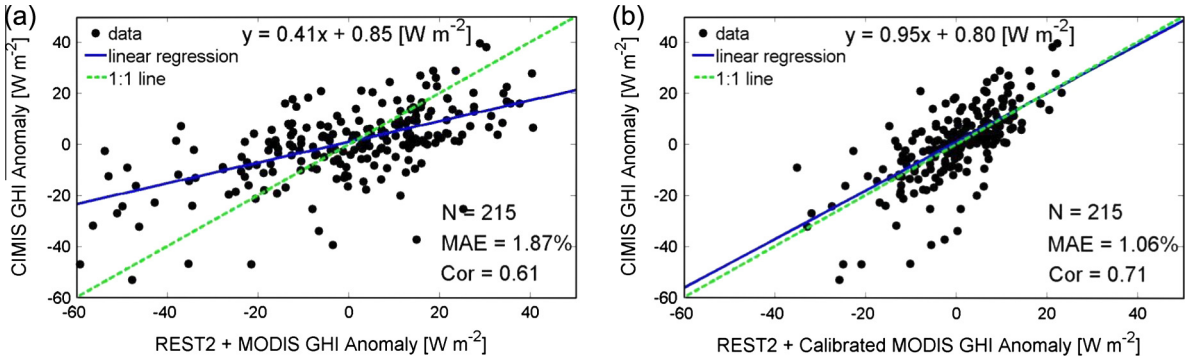

Fig. 6. Comparison of GHI Anomaly for uncalibrated MODIS AOD and PW (a) and calibrated MODIS data (b) for MODIS pixel #16 and CIMIS station 167 at Tracy.

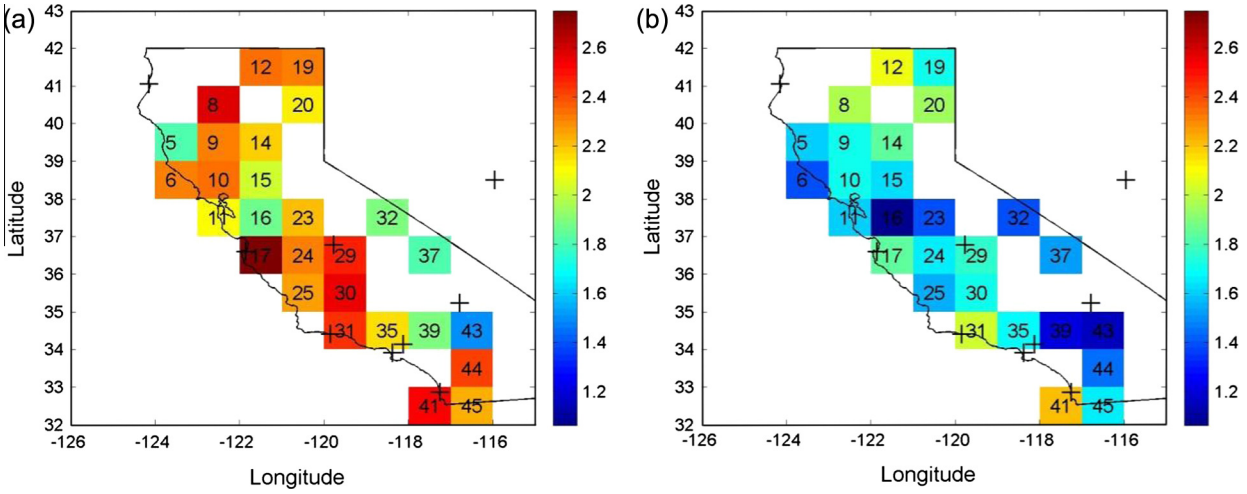

Fig. 7. Comparison of rMAE of GHI anomaly for uncalibrated (a) and calibrated MODIS AOD and PW (b). White areas indicate pixels without high quality CIMIS stations. Units of errors are %. + indicate AERONET sites. Number in boxes is the MODIS pixel number.

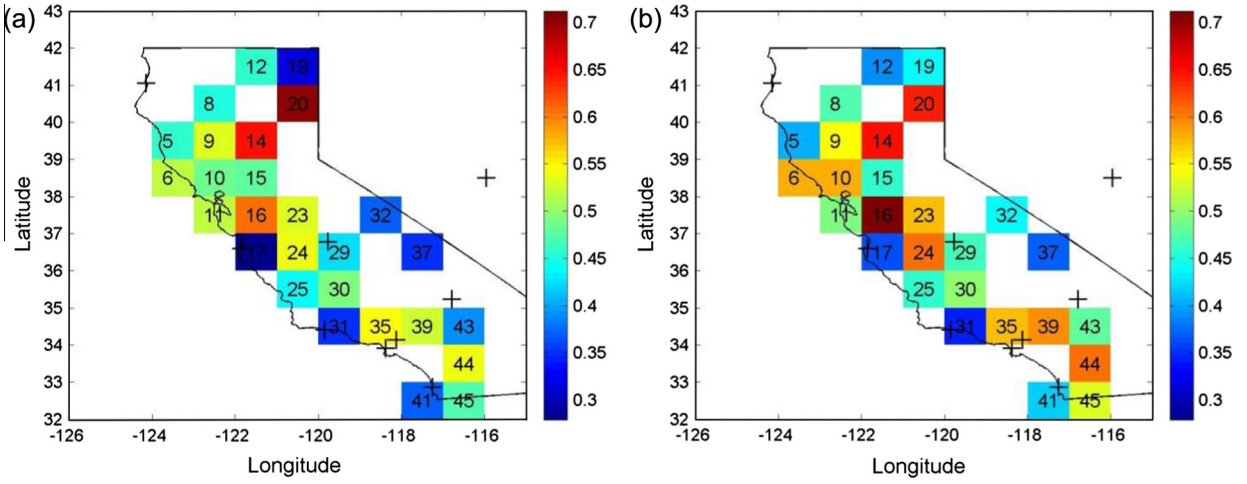

Fig. 8. Comparison of correlation coefficient of GHI anomaly for uncalibrated MODIS AOD and PW (a) and calibrated MODIS data (b). White areas indicate pixels without high quality CIMIS stations. + indicate AERONET sites. Number in boxes is the MODIS pixel number.

calibrated MODIS AOD and PW. Similarly, for most other MODIS pixels, the erroneous enhancement of AOD and PW causes the REST2 + uncalibrated MODIS predicted GHI anomaly to have a larger variance than the measured GHI anomaly. Calibration moves the GHI anomaly data close to the 1:1 line resulting in a large

reduction in mean absolute errors (on average 27%, Table 8.1) and a small improvement in correlation coefficients (from 0.50 to 0.53, on average, Table 8.2). For Ineichen, the calibration of MODIS data reduces rMAE by almost 31% and increases the correlation coefficients by 10%, on average.

Figs. 7 and 8, which spatially display the error metrics of GHI from Table 8 for uncalibrated and calibrated MODIS input data, confirm that calibration of AOD and PW reduces rMAEs and increases correlation coefficients, but spatial patterns or other determinants of errors did not emerge from this analysis.

5.3. Direct normal irradiance anomaly

While Ineichen is a clear sky model for GHI only, for McClear DNI can be calculated using the GHI and clear sky diffuse irradiance. Fig. 9 and Table 9 compare ISIS and NREL measurements against REST2 predicted DNI anomaly for uncalibrated and calibrated MODIS input data. Calibration reduces rMAE of the DNI anomaly by 45%, on average (Table 9). The non-anomaly DNI results are compared in Tables A-4 and A-5 (Appendix A). While REST2 + calibrated MODIS outperforms the other models, the REST2 + uncalibrated MODIS, McClear and REST2 + MACC show nearly the same overall performance, which indicates that the results are most sensitive to the quality of the input data.

6. Discussion of REST2 and MODIS errors in predicting GHI and DNI

The GHI and DNI anomaly errors may come from a variety of sources. In Section 3 we showed that there are errors in MODIS daily AOD and PW when compared to AERONET. The linear calibration of MODIS AOD and PW significantly improved the GHI and DNI anomaly errors, but random MODIS errors remain that are caused by spatial heterogeneity in AOD and PW fields over the 100×100 km MODIS L3 pixels, random errors in MODIS measurements, and assumptions in the postprocessing algorithms. In addition the MODIS Angstrom exponent fails to provide quantitative information about aerosol size over land (Levy et al., 2010). Other error sources are the assumption of REST2 inputs other than aerosols and water, such as ground albedo, total ozone abundance, total nitrogen dioxide abundance and aerosol single scattering albedo for both REST2 bands (Table 1).

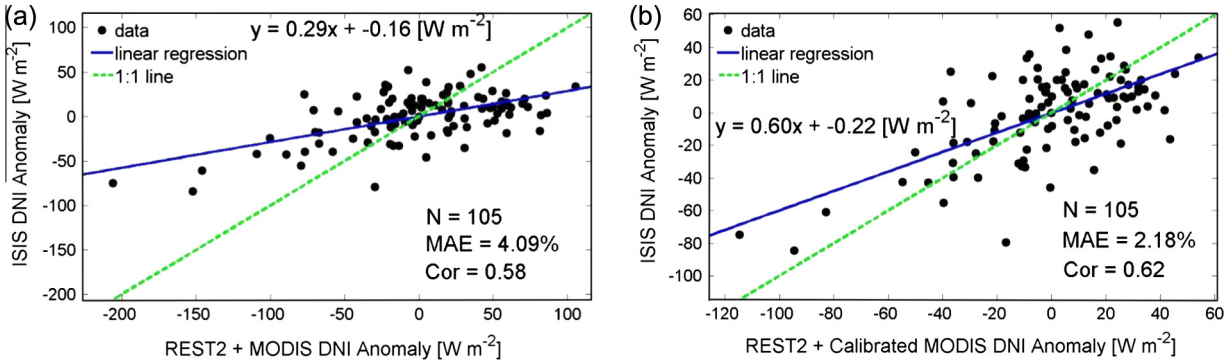

Fig. 9. Comparison of REST2 predicted DNI anomaly for uncalibrated (left) and calibrated MODIS AOD and PW (right) for MODIS pixel #29 and ISIS site (Hanford) in 2011. As more quality control rules were applied in the DNI analysis, generally less data points remain for the DNI validation compared to the GHI validations (e.g. Fig. 6).

Table 9
rMAE and Correlation coefficient of REST2 (columns 5, 6, 8–10 and 12) and McClear (columns 7 and 11) predicted DNI anomalies against NREL and ISIS measured DNI anomalies. Anomalies were calculated by subtracting 15 day moving averages (Eq. (9)). All errors are relative errors normalized by annual average ground measured DNI.

#	Name	AERONET	Distance (km)	REST2 + MODIS		McClear	REST2 + MACC	REST2 + MODIS		McClear	REST2 + MACC
				rMAE (%)	cal_rMAE (%)	rMAE (%)	rMAE (%)	Cor	cal_Cor	Cor	Cor
2	HSU	Trinidad Head	55	1.97	1.84	2.53	2.64	0.81	0.66	0.61	0.60
15	SMUD	Fresno	23	2.90	1.77	3.09	3.30	0.51	0.59	0.51	0.51
36	LMU	UCSB	52	6.78	2.61	3.66	3.92	0.25	0.28	0.39	0.38
46	UNLV	Goldstone	73	3.13	1.88	3.98	4.39	0.58	0.65	0.50	0.49
29	Hanford	Fresno	24	4.09	2.18	2.85	2.95	0.58	0.62	0.65	0.64
Max				6.78	2.61	3.98	4.39	0.81	0.66	0.65	0.64
Min				1.97	1.77	2.53	2.64	0.25	0.28	0.39	0.38
Average				3.78	2.06	3.22	3.44	0.54	0.56	0.53	0.52

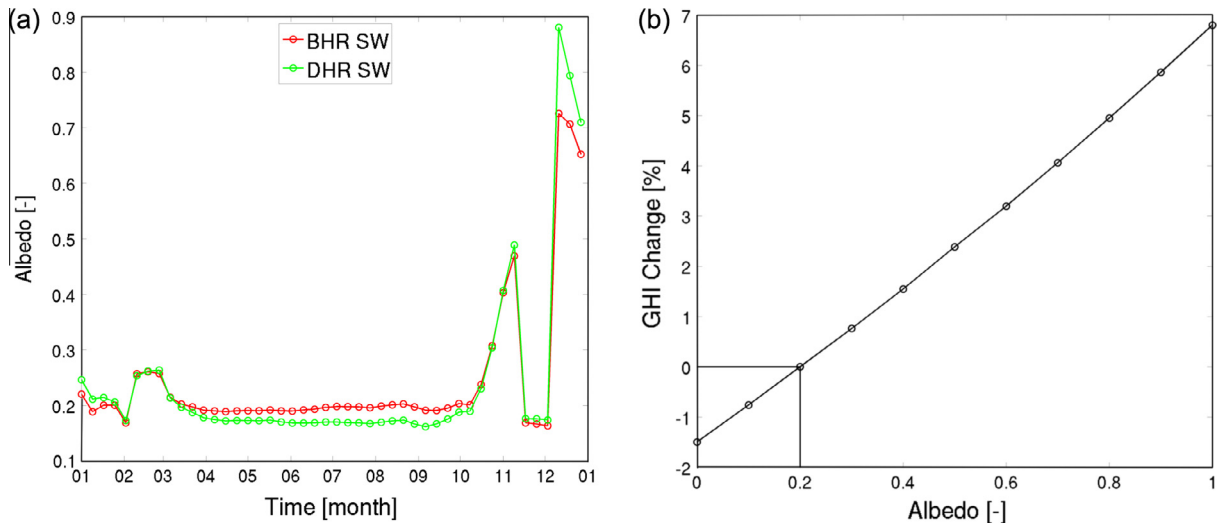

Fig. 10. (a) Directional-hemispherical reflectance (DHR) and bi-hemispherical reflectance (BHR) for the broadband solar spectrum for CIMIS station #57 in 2010 from the GlobAlbedo project (Muller et al., 2012). (b) Sensitivity of REST2 predicted GHI to land surface albedo for Angstrom turbidity coefficient, Angstrom Exponent, PW, surface pressure and SZA of 0.03, 0.629, 0.75 cm, 880 mb and 67°. GHI change was calculated relative to the reference GHI with albedo equals 0.2.

For example, ground albedo exhibits spatial and temporal variability due to land use change and rain or snow. Especially, the appearance of snow during winter time in the areas of three CIMIS stations (43, 57 and 183) leads to sudden and large changes in ground albedo. Fig. 10a shows the timeseries of directional-hemispherical reflectance (DHR) and bi-hemispherical reflectance (BHR) for solar spectrum shortwave (SW, 0.4-3 μm) for CIMIS station #57. Note that the blue-sky (actual) albedo is the interpolation between BHR and DHR using He et al. (2012).

$$\alpha_{\text{blue}} = f_{\text{dif}}\alpha_{\text{ws}} + (1 - f_{\text{dif}})\alpha_{\text{bs}}, \tag{10}$$

where α_{blue}, α_{ws} and α_{bs} are the blue-sky, black-sky and white-sky albedo, and f_{dif} is the portion of diffuse illumination, which is a function of optical depth, solar zenith angle, aerosol type, and band. Over the albedo range encountered at snowy sites (0.1–0.9), REST2 GHI varies close to linearly and by about 7% for CIMIS station #57 for Angstrom turbidity coefficient, Angstrom Exponent, PW, surface pressure and SZA of 0.03, 0.629, 0.75 cm, 880 mb and 67°, respectively (Fig. 10b). Albedo changes during the remainder of the season (0.1–0.3) only causes less than 1% change in REST2 GHI. Therefore, we suggest that measured albedo should be used for snowy sites, while the default albedo is sufficiently accurate for other sites where snow is not observed and albedo changes are more gradual and of smaller amplitude.

7. Comparison of non-anomaly error metrics against the literature

The present study needs to be placed in the context of prior applications of REST2 and other clear sky models. Utilizing local ground measured data for all REST2 inputs (the best, albeit rare scenario) Gueymard (2008) tested the performance of REST2 predictions of GHI and DNI using a set of 30 individual measurements obtained at the Southern Great Plain (SGP) site of Billings, Oklahoma, USA. MBE and RMSE of GHI were 0% and 0.6% respectively, and MBE and RMSE of DNI were 0.3% and 0.8%. Gueymard (2010) validated five models to predict clear sky DNI with high quality datasets including aerosol and water vapor measurements by sun photometers as inputs against high quality measured clear-sky irradiance data. Under such ideal conditions, the REST2, METSTAT and Ineichen clear sky models achieved accuracy comparable to that of a first-class pyrheliometer (maximum rRMSE for DNI are 2.0%, 5.6% and 4.7% respectively). Rizwan et al. (2010) used the REST2 model with precipitable water calculated from measured relative humidity and atmospheric temperature to estimate the solar resource at four stations in India and the maximum REST2 rRMSE for GHI was 3.4%.

In this paper, the error metrics of both GHI and DNI in Tables A-1–A-5 (Appendix A) are larger than previously published results, because satellite-derived inputs to REST2 are much less accurate. Other investigators who used satellite derived inputs include Lefèvre et al. (2013), who validated McClear irradiances with MODIS and MACC as inputs against 1 min measurements under clear sky conditions at Baseline Surface Radiation Network (BSRN) stations in various climates. For GHI, the bias was between −6 and 25 W m^{-2}, and RMSE ranged between 20 W m^{-2} (3% of the mean GHI) and 36 W m^{-2} (5%). The DNI bias ranged between −48 and 33 W m^{-2} and RMSE ranged between 33 W m^{-2} (5%) and 64 W m^{-2} (10%). The tables in Appendix A presents accuracies consistent with those of Lefèvre et al. (2013). Ruiz-Arias et al. (2013) found that MODIS L3 AOD is of sufficient quality to produce accurate

enough GHI at the regional scale introducing an uncertainty of approximately 15% in DNI and less than 5% for GHI (for AOD smaller than 0.5). Comparing Tables 8 with 9 shows that relative error of DNI anomaly is generally larger than that of GHI anomaly, consistent with the findings by Ruiz et al. (2013).

8. Conclusions

MODIS L3 daily AOD and PW were compared against AERONET ground measurements in California. Large biases were observed especially in AOD that were removed using a linear regression against AERONET observations in a similar climate zone. Validation against ground stations demonstrated that bias and random errors of REST2 GHI and DNI prediction are improved when calibrated MODIS L3 data is input to REST2. The improvements were quantified using the GHI and DNI anomalies thereby removing the issue of the always high correlation due to annual and daily cycle of solar angles. The daily REST2 + calibrated MODIS product also favorably compared against the anomaly obtained from the (a) REST2 with MACC reanalysis data, (b) Ineichen model with (i) uncalibrated MODIS L3 data, (ii) the monthly climatological SoDa database for Linke turbidity, and (iii) MACC reanalysis data, as well as (c) McClear. The Ineichen + calibrated MODIS achieved similar accuracy to REST2 + calibrated MODIS, which indicates that the quality of the input data is a larger differentiator than the clear sky model. Our new operationalizable REST2 + calibrated MODIS product can improve the accuracy of satellite-based clear sky solar resource assessment and forecasting to an average rMBE of 1.5% and rMAE of anomalies of 1.6%. Since most semi-empirical satellite models require clear sky irradiance as a baseline and in California clear sky differences can contribute substantially to bias errors in satellite models (Jamaly et al., 2012), solar resources can be assessed more accurately and economically over a large region.

Acknowledgements

The authors would like to thank (i) the AERONET, CIMIS, ISIS, and NREL science teams for establishing and maintaining the field measurements used in this paper; (ii) MODIS and MACC reanalysis science teams for the processing and public availability of the aerosol and water vapor products; and (iii) funding from the California Public Utilities Commission California Solar Initiative.

Appendix A. Non-anomaly GHI and DNI validation

The appendix provides validation data for the REST2 GHI and DNI before running means are removed to obtain anomalies. Comparison against CIMIS data shows generally positive bias errors, which may be an artifact of insufficient maintenance such as soiling (Geuder and Quaschning, 2006; Mejia and Kleissl, 2013) of the CIMIS

Table A-1
rMBE of REST2 (columns 5, 6 and 11), Ineichen (columns 7–9, and 12) and McClear (column 10) predicted GHI against NREL and ISSI measured GHI. Climatological SoDa data and MACC data are also investigated as alternative inputs. All errors are relative errors normalized by the annual average GHI for each ground station.

#	ID	AERONET	Distance (km)	REST2 + MODIS		Ineichen + MODIS		Ineichen + SoDa	McClear	REST2 + MACC	Ineichen + MACC
				rMBE (%)	cal_rMBE (%)	rMBE (%)	cal_rMBE (%)	rMBE (%)	rMBE (%)	rMBE (%)	rMBE (%)
2	HSU	Trinidad Head	55	3.28	5.30	2.21	3.04	0.07	7.52	3.18	0.60
15	SMUD	Fresno	23	3.94	1.73	2.76	0.60	−0.76	6.10	2.49	0.18
36	LMU	UCSB	52	−5.35	1.26	−6.60	−0.32	−5.85	1.55	−2.04	−4.37
46	UNLV	Goldstone	73	−10.03	1.11	−13.63	−1.17	−3.79	−0.38	−3.84	−7.12
29	Hanford	Fresno	24	−1.49	−1.72	−2.93	−3.05	−6.19	1.94	−2.41	−4.54
Max				−10.03	5.30	−13.63	−3.05	−6.19	7.52	−3.84	−7.12
Min				1.49	1.11	2.21	0.32	0.07	0.38	2.04	0.18
Average				−1.93	1.54	−3.64	−0.18	−3.30	3.34	−0.52	−3.05

Table A-2
rMAE of REST2 (columns 5, 6 and 11), Ineichen (columns 7 to 9, and 12) and McClear (column 10) predicted GHI against NREL and ISIS measured GHI.

#	ID	AERONET	Distance (km)	REST2 + MODIS		Ineichen + MODIS		Ineichen + SoDa	McClear	REST2 + MACC	Ineichen + MACC
				rMAE (%)	cal_rMAE (%)	rMAE (%)	cal_rMAE (%)	rMAE (%)	rMAE (%)	rMAE (%)	rMAE (%)
2	HSU	Trinidad Head	55	3.58	5.30	2.83	3.11	2.10	7.68	3.64	2.54
15	SMUD	Fresno	23	4.23	2.51	3.33	2.06	1.68	6.18	3.42	2.37
36	LMU	UCSB	52	5.44	2.16	6.66	1.87	5.85	2.37	2.78	4.39
46	UNLV	Goldstone	73	10.03	1.61	13.63	1.84	3.95	1.87	3.92	7.12
29	Hanford	Fresno	24	2.74	2.31	3.40	3.21	6.20	3.16	3.21	4.88
Max				10.03	5.30	13.63	3.21	6.20	7.68	3.92	7.12
Min				2.74	1.61	2.83	1.84	1.68	1.87	2.78	2.37
Average				5.20	2.78	5.97	2.42	3.96	4.25	3.39	4.26

Table A-3
rRMSE[a] of REST2 (columns 5, 6 and 11), Ineichen (columns 7–9, and 12) and McClear (column 10) predicted GHI against NREL and ISIS measured GHI.

#	ID	AERONET	Distance (km)	REST2 + MODIS		Ineichen + MODIS		Ineichen + SoDa	McClear	REST2 + MACC	Ineichen + MACC
				rRMSE (%)	cal_rRMSE (%)	rRMSE (%)	cal_rRMSE (%)	rRMSE (%)	rRMSE (%)	rRMSE (%)	rRMSE (%)
2	HSU	Trinidad Head	55	4.08	5.71	3.59	3.65	2.60	7.93	4.32	3.26
15	SMUD	Fresno	23	4.90	2.85	3.88	2.39	2.18	6.56	3.96	3.04
36	LMU	UCSB	52	6.83	2.67	8.87	2.20	6.30	2.86	3.39	5.20
46	UNLV	Goldstone	73	10.33	1.94	14.18	2.33	4.55	2.40	4.51	7.82
29	Hanford	Fresno	24	3.59	2.90	4.25	3.81	6.80	4.10	3.93	5.65
Max				10.33	5.71	14.18	3.81	6.80	7.93	4.51	7.82
Min				3.59	1.94	3.59	2.20	2.18	2.40	3.39	3.04
Average				5.94	3.21	6.95	2.88	4.48	4.47	4.02	4.99

[a] $\mathrm{rRMSE} = \frac{\sqrt[2]{\frac{1}{N}\sum_{i=1}^{N}\left(\frac{\mathrm{GHI}_i - \mathrm{GHI}_{\mathrm{measured}}}{\mathrm{GHI}_{\mathrm{measured}}}\right)^2}}{\mathrm{GHI}_{\mathrm{annual}}}$, where GHI_i is model (such as REST2, Ineichen and McClear) predicted GHI; $\mathrm{GHI}_{\mathrm{measured}}$ is GHI measured by ground stations; $\mathrm{GHI}_{\mathrm{annual}}$ is the annual average GHI measured by ground stations.

Table A-4
rMBE and rMAE of REST2 (columns 5, 6 and 11), Ineichen (columns 7–9, and 12) and McClear (column 10) predicted DNI against NREL and ISIS measured DNI. All errors are relative errors normalized by the annual average DNI for each ground station.

#	ID	AERONET	Distance (km)	REST2 + MODIS		McClear	REST2 + MACC	REST2 + MODIS		McClear	REST2 + MACC
				rMBE (%)	cal_rMBE (%)	rMBE (%)	rMBE (%)	rMAE (%)	cal_rMAE (%)	rMAE (%)	rMAE (%)
2	HSU	Trinidad Head	55	0.54	2.59	4.05	−0.95	3.71	4.23	5.43	5.01
15	SMUD	Fresno	23	−0.65	−5.71	−0.24	−5.21	3.49	5.85	3.34	5.71
36	LMU	UCSB	52	−11.66	1.49	−1.60	−7.08	11.77	3.87	5.47	8.24
46	UNLV	Goldstone	73	−26.28	2.35	−5.17	−9.80	26.28	2.78	6.26	10.03
29	Hanford	Fresno	24	1.76	1.12	4.11	−1.91	4.78	2.77	5.06	4.01
Max				−26.28	−5.71	−5.17	−9.80	26.28	5.85	6.26	10.03
Min				0.54	1.12	0.24	0.95	3.49	2.77	3.34	4.01
Average				−7.26	0.37	0.23	−4.99	10.00	3.90	5.11	6.60

Table A-5
rRMSE and Cor of REST2 (columns 5, 6 and 11), Ineichen (columns 7–9, and 12) and McClear (column 10) predicted DNI against NREL and ISIS measured DNI.

#	ID	AERONET	Distance (km)	REST2 + MODIS		McClear	REST2 + MACC	REST2 + MODIS		McClear	REST2 + MACC
				rRMSE (%)	cal_rRMSE (%)	rRMSE (%)	rRMSE (%)	Cor	cal_Cor	Cor	Cor
2	HSU	Trinidad Head	55	4.71	5.10	6.51	6.18	0.78	0.64	0.66	0.62
15	SMUD	Fresno	23	4.52	6.70	4.89	7.30	0.75	0.75	0.69	0.71
36	LMU	UCSB	52	15.83	4.95	7.31	10.93	0.51	0.33	0.29	0.23
46	UNLV	Goldstone	73	26.68	3.56	8.25	12.21	0.60	0.73	0.59	0.56
29	Hanford	Fresno	24	5.77	3.46	6.60	5.41	0.70	0.77	0.59	0.62
Max				26.68	6.70	8.25	12.21	0.78	0.77	0.69	0.71
Min				4.52	3.46	4.89	5.41	0.51	0.33	0.29	0.23
Average				11.50	4.75	6.71	8.41	0.67	0.64	0.56	0.55

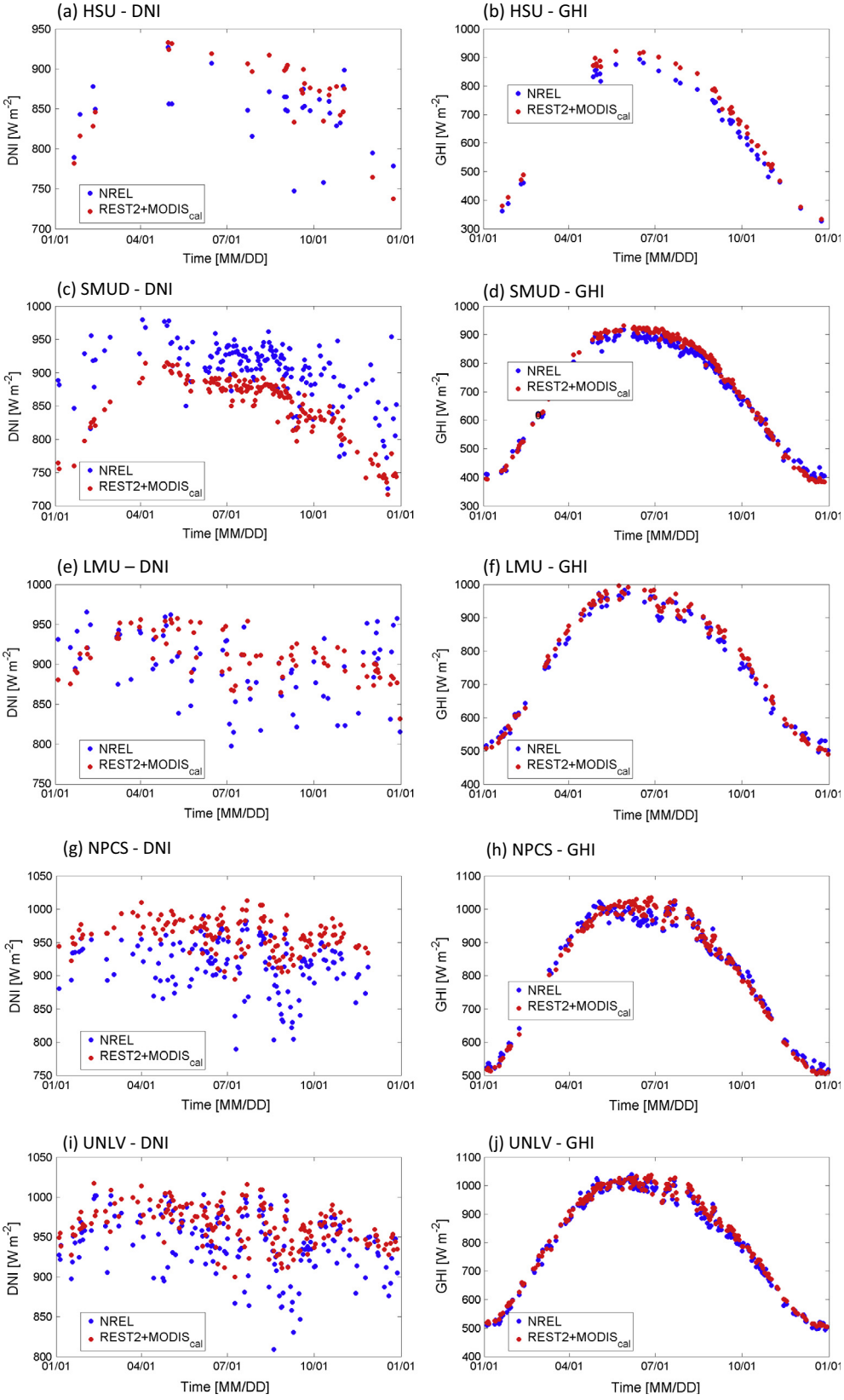

Fig. B-1. Timeseries of NREL measured and REST2 + calibrated MODIS predicted DNI (a, c, e, g, i) and GHI (b, d, f, h, j) for calibrated MODIS AOD at 0.55 μm and PW on every clear day in 2011. (a, b) MODIS pixel #2 and HSU station; (c, d) MODIS pixel #15 and SMUD station; (e, f) MODIS pixel #36 and LMU station; (g, h) MODIS pixel #46 and NPCS station; (i, j) MODIS pixel #46 and UNLV station.

stations that results in underestimating solar irradiance by a few percent. Given the less rigorous quality of CIMIS data, the results are more questionable and not provided.

Tables A-1–A-3 (A-4–A-5) validate the GHI (DNI) from REST2 against NREL and ISIS measured GHI (DNI). rMBE in Table A-1 shows that with uncalibrated MODIS data, the REST2 and Ineichen underestimate GHI for four out of six stations. The general decrease in the GHI errors after calibration of MODIS data is consistent with the fact that MODIS usually overestimates AOD compared to AERONET. Since calibration decreases MODIS AOD the REST2 predicted GHI increases compared to NREL and ISIS measured GHI decreasing errors. On the other hand, for the SMUD station, where rMBE of REST2 + MODIS and Ineichen + MODIS is positive, GHI rMBE and rMAE also decrease after MODIS calibration, probably because Fresno is the only AERONET site where MODIS underestimated PW compared to AERONET. Since the decrease in GHI related to calibration of MODIS PW dominates over the increase related to calibrated MODIS AOD, GHI errors decrease for SMUD. For the same reason, GHI errors increase for the ISIS station Hanford which originally has negative GHI rMBE. Tables A-1–A-3 demonstrate that Ineichen + calibrated MODIS predict GHI most accurately, REST2 + calibrated MODIS is slightly less accurate, and Ineichen + uncalibrated MODIS is of the lowest accuracy as measured by GHI rMAE. REST2 + MACC is shown to have the best performance excluding the REST2 and Ineichen + calibrated MODIS, indicating that better quality PW data is more critical than AOD in modeling clear sky GHI in California given that transmission of clear sky GHI is more determined by PW than generally small AOD.

Tables A-4 and A-5 compare the REST2 predicted DNI with NREL and ISIS DNI. Uncalibrated DNI is underestimated significantly for LMU and UNLV compared to the other 3 sites possibly due to the relatively large positive bias in uncalibrated AOD from the MODIS pixels near Goldstone (Table 5) and uncalibrated PW from MODIS pixels near UCSB (Table 6). DNI is much more sensitive to AOD than GHI. Similar to the GHI comparison, the REST2 + calibrated MODIS still shows the smallest rMAE. McClear comes in second in terms of the overall performance.

Appendix B. Ground station data quality assessment

Since ground stations need to be well maintained to provide accurate data, several data quality checks were conducted. Soiling can cause overestimation by clear sky models. While soiling typically occurs slowly and is automatically corrected through the anomaly method, fast soiling has the potential to affect anomalies. Google Earth was used to determine whether surface cover near the site would have potential for fast soiling. The NPCS site is located at the Nevada Power Clark Station which creates potential for soiling from air pollution. Hanford is situated in an agriculture area which creates potential for soiling. The other sites were not found to be near sources of fast soiling. Since maintenance records were lacking at NPCS and either high AOD days or soiling days occurred around July 1st, the NPCS station was excluded in the paper.

Further, maintenance records were examined. Afshin Andreas, Senior Scientist at National Renewable Energy Laboratory (NREL), provided point of contacts for all NREL associated sites. The site hosts who responded provided the following records:

LMU: Jeremy Pal, Associate Professor at Department of Civil Engineering and Environmental Science, Loyola Marymount University, indicated that the data before May 2012 was reliable. Based on the LMU maintenance record, maintenance was performed at least once a month in 2011. Fig. B-1f confirms that the data appear to be of high quality as observation and model data follow the same trend.

UNLV: Aaron Sahm, Research Engineer at University of Nevada at Las Vegas, provided a cleaning log that documents cleaning at least four times a month in 2011. The model data also captured the observed data very well.

Hanford: John Augustine, scientist at NOAA Earth System Research Laboratory Global Monitoring Division,

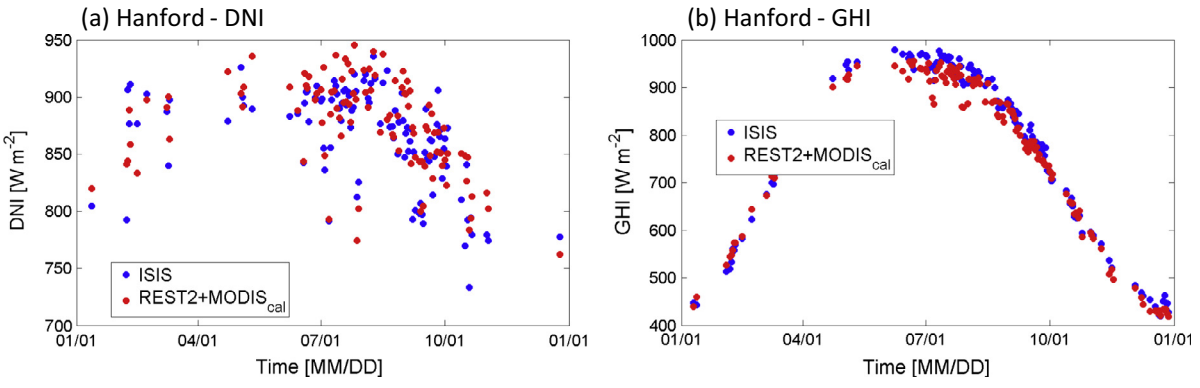

Fig. B-2. Timeseries of ISIS measured and REST2 + calibrated MODIS predicted DNI (a) and GHI (b) for calibrated MODIS AOD at 0.55 μm and PW at MODIS pixel #29 and Hanford station on every clear day in 2011.

mentioned that the local hosts at the National Weather Service clean the instruments on a weekly basis and did quasi-annual site visits to exchange instruments with freshly calibrated units, clean the equipment, and conduct preventative maintenance by replacing equipment regularly. For example, ventilator fans, data loggers are replaced on a three-year cycle.

Figs. B-1 and B-2 show DNI and GHI timeseries at 10:30 on every clear day in 2011. Overall, there is no obvious fast soiling event or maintenance issues observed for the five stations (HSU, SMUD, LMU, UNLV and Hanford) above in 2011.

References

Anderson, G.P., Clough, S.A., Kneizys, F.X., Chetwynd, J.H., Shettle, E.P., 1989. AFGL atmospheric constituent profiles (0–120 km). Environ. Res. Pap.

Bellouin, N., Quaas, J., Morcrette, J.-J., Boucher, O., 2013. Estimates of aerosol radiative forcing from the MACC re-analysis. Atmos. Chem. Phys. 13, 2045–2062. http://dx.doi.org/10.5194/acp-13-2045-2013.

Benedetti, A., Morcrette, J.-J., Boucher, O., Dethof, A., Engelen, R.J., Fisher, M., Flentje, H., Huneeus, N., Jones, L., Kaiser, J.W., Kinne, S., Mangold, A., Razinger, M., Simmons, a.J., Suttie, M., 2009. Aerosol analysis and forecast in the European centre for medium-range weather forecasts integrated forecast system: 2. Data assimilation. J. Geophys. Res. 114. http://dx.doi.org/10.1029/2008JD011115.

Benedictow, A., Blechschmidt, A.-M., Bouarar, I., Botek, E., Chabrillat, S., Christophe, Y., Cuevas, E., Clark, H., Flentje, H., Gaudel, A., Griesfeller, J., Huijnen, V., Huneeus, N., Jones, L., Kapsomenakis, J., Kinne, S., Langerock, B., Lefever, K., Razinger, M., Richter, A., Schulz, M., Thomas, W., Thouret, V., Vrekoussis, M., Wagner, A., Zerefos, C., 2014. Validation report of the MACC reanalysis of global atmospheric composition: period 2003–2012. Tech. Rep., MACC-II Project.

Berk, A., Bornstein, L.S., David, C., Street, S.B., 1989. MODTRAN: A Moderate Resolution Model for LOWTRAN 7. Burlington, Massachusetts. Final Report GL-TR-89- 0122, Geophysics Laboratory, U.S. Air Force Systems Command, Hanscomb AFB, Massachusetts, USA.

Blanc, P., Gschwind, B., Lefèvre, M., Wald, L., 2014. Twelve monthly maps of ground albedo parameters derived from MODIS data sets. In: Geoscience and Remote Sensing Symposium (IGARSS). Quebec City, QC, pp. 3270–3272. doi:http://dx.doi.org/10.1109/IGARSS.2014.6947177.

Chou, M., Suarez, M., 1994. An efficient thermal infrared radiation parameterization for use in general circulation models. NASA Tech. Memo.

CIMIS Overview (WWW Document), n.d. URL <http://wwwcimis.water.ca.gov/cimis/infoGenCimisOverview.jsp;jsessionid=84946C8255FB2216A77F9567B5FEC9BA> (accessed 27.02.13).

CIMIS Sensor Specifications (WWW Document), n.d. URL <http://wwwcimis.water.ca.gov/Stations.aspx> (accessed 27.02.13).

CIMIS Maintenance (WWW Document), n.d. URL <http://www.cimis.water.ca.gov/Stations.aspx> (accessed 21.01.15).

Eching, S., Moellenberndt, D., 1998. Technical elements of CIMIS, the California Irrigation Management Information System, State of California, Resources Agency, Dept. of Water Resources, Division of Planning and Local Assistance, Sacramento, CA.

ECMWF (WWW Document), 2014. URL <http://old.ecmwf.int/products/data/archive/data_faq.html> (accessed 25.10.14).

Gao, B.-C., 2003. Water vapor retrievals using Moderate Resolution Imaging Spectroradiometer (MODIS) near-infrared channels. J. Geophys. Res. 108, 4389. http://dx.doi.org/10.1029/2002JD003023.

Gao, B.-C., Kaufman, Y.J., 2003. Water vapor retrievals using Moderate Resolution Imaging Spectroradiometer (MODIS) near-infrared channels. J. Geophys. Res. 108, 4389. http://dx.doi.org/10.1029/2002JD003023.

Geuder, N., Quaschning, V., 2006. Soiling of irradiation sensors and methods for soiling correction. Sol. Energy 80, 1402–1409. http://dx.doi.org/10.1016/j.solener.2006.06.001.

Geuder, N., Pulvermüllerb, B., Vorbrugg, O., 2008. Corrections for Rotating Shadowband Pyranometers for Solar Resource Assessment. SPIES Optics + Photonics, San Diego, pp. 1–12.

Geuder, N., Janotte, N., Wilbert, S., 2009. Precise measurements of solar beam irradiance through improved sensor calibration. SolarPACES, 1–8.

Gueymard, C.A., 2003. Direct solar transmittance and irradiance predictions with broadband models. Part II: Validation with high-quality measurements. Sol. Energy 74, 381–395.

Gueymard, C.A., 2008. REST2: High-performance solar radiation model for cloudless-sky irradiance, illuminance, and photosynthetically active radiation – validation with a benchmark dataset. Sol. Energy 82, 272–285. http://dx.doi.org/10.1016/j.solener.2007.04.008.

Gueymard, C.A., 2010. Progress in Direct Irradiance Modeling and Validation. ASES Annual Conference, Phoenix, AZ, USA.

Gueymard, C.A., 2012a. A globally calibrated aerosol optical depth gridded dataset for improved solar irradiance predictions. Geophys. Res. Abstr. 14, 11706.

Gueymard, C.A., 2012b. Clear-sky irradiance predictions for solar resource mapping and large-scale applications: improved validation methodology and detailed performance analysis of 18 broadband radiative models. Sol. Energy 86, 2145–2169. http://dx.doi.org/10.1016/j.solener.2011.11.011.

Gueymard, C.A., 2012c. Temporal variability in direct and global irradiance at various time scales as affected by aerosols. Sol. Energy 86, 3544–3553. http://dx.doi.org/10.1016/j.solener.2012.01.013.

Gueymard, C.A., Thevenard, D., 2009. Monthly average clear-sky broadband irradiance database for worldwide solar heat gain and building cooling load calculations. Sol. Energy 83, 1998–2018. http://dx.doi.org/10.1016/j.solener.2009.07.011.

Gueymard, C.A., Wilcox, S.M., 2011. Assessment of spatial and temporal variability in the US solar resource from radiometric measurements and predictions from models using ground-based or satellite data. Sol. Energy 85, 1068–1084. http://dx.doi.org/10.1016/j.solener.2011.02.030.

Gurtuna, O., Prevot, A., 2011. An overview of solar resource assessment using meteorological satellite data. In: Proc. 5th Int. Conf. Recent Adv. Sp. Technol. – RAST2011, pp. 209–212. doi:http://dx.doi.org/10.1109/RAST.2011.5966825.

Hauser, A., Oesch, D., Foppa, N., 2005a. Aerosol optical depth over land: comparing AERONET, AVHRR and MODIS. Geophys. Res. Lett. 32. http://dx.doi.org/10.1029/2005GL023579.

Hauser, A., Oesch, D., Foppa, N., Wunderle, S., 2005b. NOAA AVHRR derived aerosol optical depth over land. J. Geophys. Res. 110. http://dx.doi.org/10.1029/2004JD005439.

He, T., Liang, S., Wang, D., Wu, H., Yu, Y., Wang, J., 2012. Estimation of surface albedo and directional reflectance from Moderate Resolution Imaging Spectroradiometer (MODIS) observations. Remote Sens. Environ. 119, 286–300. http://dx.doi.org/10.1016/j.rse.2012.01.004.

Hicks, B.B., DeLuisi, J.J., Matt, D.R., 1996. The NOAA Integrated Surface Irradiance Study (ISIS) – a new surface radiation monitoring program. Bull. Am. Meteorol. Soc. 77, 2857–2864.

Holben, B.N., Eck, T.F., Slutsker, I., Tanré, D., Buis, J.P., Setzer, A., Vermote, E., Reagan, J.A., Kaufman, Y.J., Nakajimu, T., Lavenu, F., Jnnkowiak, I., Smirnovt, A., 1998. AERONET – a federated instrument network and data archive for aerosol characterization. Remote Sens. Environ. 66, 1–16.

Holben, B.N., Tanre, D., Smirnov, A., Eck, T.F., Slutsker, I., Abuhassan, A., Newcomb, W.W., Schafer, J.S., Chatenet, B., Lavenu, F., Kaufman, Y.J., Castle, J. Vande, Setzer, A., Markham, B., Clark, D., Frouin, R., Halthore, R., Karneli, A., Neill, N.T.O., Pietras, C.,

Pinker, Voss, K., Zibordi, G., 2012. An emerging ground-based aerosol climatology: aerosol optical depth from AERONET. J. Geophys. Res. Atmos. 106, 12067–12097.
Hubanks, P.A., King, M.D., Platnick, S.A., Pincus, R.A., 2008. MODIS Atmosphere L3 Gridded Product Algorithm Theoretical Basis Document.
Ineichen, P., 2008a. Conversion function between the Linke turbidity and the atmospheric water vapor and aerosol content. Sol. Energy 82, 1095–1097. http://dx.doi.org/10.1016/j.solener.2008.04.010.
Ineichen, P., 2008b. A broadband simplified version of the Solis clear sky model. Sol. Energy 82, 758–762. http://dx.doi.org/10.1016/j.solener.2008.02.009.
Ineichen, P., Perez, R., 2002. A new airmass independent formulation for the Linke turbidity coefficient. Sol. Energy 73, 151–157. http://dx.doi.org/10.1016/S0038-092X(02)00045-2.
Jamaly, M., Bosch, J.L., Kleissl, J., 2012. Validation of SolarAnywhere Enhanced Resolution Irradiation Using Power Output of Distributed PV Systems in California. Report to the California Solar Initiative RD&D Program.
John, M., 2014. Overview of NASA's Terra satellite (WWW Document). URL <http://www2.hawaii.edu/~jmaurer/terra/> (accessed 25.09.14).
Kahn, R.A., Nelson, D.L., Garay, M.J., Levy, R.C., Bull, M.A., Diner, D.J., Martonchilk, J.V., Paradise, S.R., Hansen, E.G., Remer, L.A., 2009. MISR aerosol product attributes and statistical comparisons with MODIS. IEEE Trans. Geosci. Remote Sens. 47, 4095–4114. http://dx.doi.org/10.1109/TGRS.2009.2023115.
Kaiser, J.W., Peuch, V.-H., Benedetti, A., Boucher, O., Engelen, R.J., Holzer-Popp, T., Morcrette, J.-J., Wooster, M.J., 2012. The pre-operational GMES atmospheric service in MACC- II and its potential use of Sentinel-3 observations. In: Proceedings of the 3rd MERIS/(A)ATSR and OCLI-SLSTR (Sentinel-3) Preparatory Workshop. ESA-ESRIN, Frascati, Italy.
King, D.L., Myers, D.R., 1997. Silicon-photodiode pyranometers: operational characteristics, historical experiences, and new calibration procedures. In: Photovoltaic Specialists Conference, Anaheim, CA, pp. 1285–1288. doi:http://dx.doi.org/10.1109/PVSC.1997.654323.
King, M.D., Menzel, W.P., Kaufman, Y.J., Tanré, D., Gao, B., Platnick, S., Ackerman, S.A., Remer, L.A., Pincus, R., Hubanks, P.A., 2003. Cloud and aerosol properties, precipitable water, and profiles of temperature and water vapor from MODIS. IEEE Trans. Geosci. Remote Sens. 41, 442–458.
Lefèvre, M., Oumbe, a., Blanc, P., Espinar, B., Gschwind, B., Qu, Z., Wald, L., Schroedter-Homscheidt, M., Hoyer-Klick, C., Arola, a., Benedetti, a., Kaiser, J.W., Morcrette, J.-J., 2013. McClear: a new model estimating downwelling solar radiation at ground level in clear-sky conditions. Atmos. Meas. Tech. 6, 2403–2418. http://dx.doi.org/10.5194/amt-6-2403-2013.
Levy, R.C., Remer, L.A., Kleidman, R.G., Mattoo, S., Ichoku, C., Kahn, R., Eck, T.F., 2010. Global evaluation of the Collection 5 MODIS dark-target aerosol products over land. Atmos. Chem. Phys. 10, 10399–10420. http://dx.doi.org/10.5194/acp-10-10399-2010.
Li, Z., Muller, J.-P., Cross, P., 2003. Comparison of precipitable water vapor derived from radiosonde, GPS, and moderate-resolution imaging spectroradiometer measurements. J. Geophys. Res. 108. http://dx.doi.org/10.1029/2003JD003372.
Long, C.N., Ackerman, T.P., 2000. Identification of clear skies from broadband pyranometer measurements and calculation of downwelling shortwave cloud effects. J. Geophys. Res. 105, 15609–15626. http://dx.doi.org/10.1029/2000JD900077.
Luoma, J., Kleissl, J., 2012. Summary of Quality Control for 2010 CIMIS Data, Internal Report.
MACC (WWW Document), n.d. URL <http://apps.ecmwf.int/datasets/-data/macc_reanalysis/> (accessed 24.09.14).
Meek, D.W., Hatfield, J.L., 1994. Data quality checking for single station meteorological databases. Agric. For. Meteorol. 69, 85–109. http://dx.doi.org/10.1016/0168-1923(94)90083-3.
Mejia, F.A., Kleissl, J., 2013. Soiling losses for solar photovoltaic systems in California. Sol. Energy 95, 357–363.
Miller, S.D., Heidinger, A.K., Sengupta, M., 2013. Physically-based satellite methods. Keywords: satellite observing systems, cloud retrieval, GOES-R, spectrum, aerosol retrieval, cloud height, ISCCP, SASRAB, PATMOS-x. In: Kleissl, J. (Ed.), Solar Energy Forecasting and Resource Assessment. Elsevier.
Mueller, R.W., Dagestad, K.F., Ineichen, P., Schroedter-Homscheidt, M., Cros, S., Dumortier, D., Kuhlemann, R., Olseth, J.A., Piernavieja, G., Reise, C., Wald, L., Heinemann, D., 2004. Rethinking satellite-based solar irradiance modelling: the SOLIS clear-sky module. Remote Sens. Environ. 91, 160–174. http://dx.doi.org/10.1016/j.rse.2004.02.009.
Muller, J.-P., López, G., Watson, G., Shane, N., Kennedy, T., Yuen, P., Lewis, P., Fischer, J., Guanter, L., Domench, C., Preusker, R., North, P., Heckel, A., Danne, O., Krämer, U., Zuhlke, M., Brockmann, G., Pinnock, S., 2012. The ESA GlobAlbedo project for mapping the earth's land surface albedo for 15 years from European sensors. In: IEEE Geoscience and Remote Sensing Symposium (IGARSS), Munich, pp. 22–27.
Pacific Gas and Electric Company, 2006. The Pacific Energy Center's Guide to: California Climate Zones and Bioclimatic Design (WWW Document).
Perez, R., Cebecauer, T., Šúri, M., 2013. Semi-empirical satellite methods. In: Kleissl, J. (Ed.), Solar Energy Forecasting and Resource Assessment. Elsevier.
Prasad, A.K., Singh, R.P., 2009. Validation of MODIS Terra, AIRS, NCEP/DOE AMIP-II Reanalysis-2, and AERONET Sun photometer derived integrated precipitable water vapor using ground-based GPS receivers over India. J. Geophys. Res. 114. http://dx.doi.org/10.1029/2008JD011230.
Remer, L.A., Kaufman, Y.J., Tanré, D., Mattoo, S., Chu, D.A., Martins, J.V., Li, R.-R., Ichoku, C., Levy, R.C., Kleidman, R.G., Eck, T.F., Vermote, E., Holben, B.N., 2005. The MODIS aerosol algorithm, products, and validation. J. Atmos. Sci. 62, 947–973. http://dx.doi.org/10.1175/JAS3385.1.
Remund, J., Wald, L., Lefevre, M., Ranchin, T., Page, J., 2003. Worldwide Linke Turbidity Information. In: Proceedings of ISES Solar World Congress, GÄteborg, Sweden.
Renné, D., George, R., Wilcox, S., Stoffel, T., Myers, D., Heimiller, D., 2008. Solar Resource Assessment (NREL/TP-581-42301), Golden CO.
Reno, M.J., Hansen, C.W., Stein, J.S., 2012. Global Horizontal Irradiance Clear Sky Models: Implementation and Analysis. Sandia Report SAND2012-2389.
Rizwan, M., Jamil, M., Kothari, D.P., 2010. Solar energy estimation using REST2 model. Int. J. Energy Environ. 1, 367–374.
Ruiz-Arias, J.A., Gueymard, C.A., Dudhia, J., Pozo-vázquez, D., 2012. Improvement of the Weather Research and Forecasting (WRF) Model for Solar Resource Assessments and Forecasts Under Clear Skies. World Renewable Energy Forum, Denver, CO.
Ruiz-Arias, J.A., Dudhia, J., Gueymard, C.A., Pozo-Vázquez, D., 2013. Assessment of the Level-3 MODIS daily aerosol optical depth in the context of surface solar radiation and numerical weather modeling. Atmos. Chem. Phys. 13, 675–692. http://dx.doi.org/10.5194/acp-13-675-2013.
Schaaf, C.B., Gao, F., Strahler, A.H., Lucht, W., Li, X., Tsang, T., Strugnell, N.C., Zhang, X., Jin, Y., Muller, J.-P., Lewis, P., Barnsley, M., Hobson, P., Disney, M., Roberts, G., Dunderdale, M., Doll, C., d'Entremont, R.P., Hu, B., Liang, S., Privette, J.L., Roy, D., 2002. First operational BRDF, albedo nadir reflectance products from MODIS. Remote Sens. Environ. 83, 135–148. http://dx.doi.org/10.1016/S0034-4257(02)00091-3.
SoDa Linke Turbidity (WWW Document), 2012. URL <http://www.soda-is.com/eng/services/linke_turbidity_info.html> (accessed 24.09.14).
Vignola, F., 2006. Removing Systematic Errors from Rotating Shadowband Pyranometer Data. The 35th ASES Annual Conference, Denver.
Vignola, F., Grover, C., Lemon, N., McMahan, A., 2012. Building a bankable solar radiation dataset. Sol. Energy 86, 2218–2229. http://dx.doi.org/10.1016/j.solener.2012.05.013.